# Scrutinizing Galaxy and AGN Evolution at its Peak Epoch with FMOS

FMOS SSP galaxy-AGN evolution team

Jan 14, 2011

**Abstract**

We propose to use the new and unique instrument FMOS to undertake a Subaru Strategic Program with the aim of fully investigating the evolution of both galaxies and active galactic nuclei (AGNs) at $1 < z < 3$, and exploring their co-evolution by obtaining rest-frame optical spectra of $\gtrsim$ 15,000 galaxies systematically. The wide field of view and high multiplexing capability of FMOS allow such studies to be performed across this critical epoch, where activity is at its peak, for the first time.

We will address the manner in which stellar mass is built up by tracing the star-formation history of the Universe through measurements of H$\alpha$ in galaxies, correcting for the effects of dust obscuration, across a wide range of environments. We will investigate the chemical evolution of galaxies through the use of well-calibrated metallicity indicators. In this manner, we will relate stellar mass, star-formation rate (SFR), metallicity, and environment across the key epoch where the cosmic SFR density peaks.

In addition to the build up of stellar mass, we will also study the growth of supermassive black holes and, in particular, quantitatively unveil obscured accretion activity which is still poorly constrained and may be missed in even the deepest X-ray surveys. Aspects of our survey are designed to study the relationship between the growth of black holes and their host galaxies by investigating the fraction of AGN among galaxies and the epoch at which black holes and their hosts stop their rapid growth phase. This connection is likely to be critical for understanding the formation of some classes of galaxies.

Our survey is naturally suited to a Japan-UK consortium as these two communities have worked together and intensively studied most of the key fields where we propose to make our observations. It is the wealth of multi-wavelength data taken by Subaru, UKIRT, *AKARI*, *Herschel*, etc., which makes our proposed science achievable.

In order to obtain the spectra of $\gtrsim$15,000 galaxies, which is two orders of magnitude larger than samples constructed so far at the redshift, we request 122 nights (accounting for overheads and weather condition) over the next five years. Solid fundamental understandings of galaxies and AGNs in the critical epoch will have world-wide legacy science value.

# 1 Overview

## 1.1 Why FMOS?: The best suited instrument to explore unresolved problems of galaxies and AGN evolution

Since the middle of the 1990s, remarkable progress has been made in studies of galaxies at high redshifts thanks to the *Hubble Space Telescope* and the advent of 8-10 m class telescopes on the ground, coupled with the development of new observational techniques. We have been able to explore aspects of the cosmic star-formation history up to $z \sim 7$ or even higher. Galaxies already exist at $z\sim$7–8, and the cosmic star-formation rate density increases gradually, comes to its peak at $z \sim 2$, and then decreases towards $z \sim 0$. The most active growth of galaxies seems to occur between $1 < z < 3$, and therefore the physical properties of the present-day galaxies seem to be established at this epoch. In fact, spiral galaxies and elliptical galaxies with similar properties to those of the present-day galaxies already exist at least up to $z \sim 1$, while no such clear counterparts are seen at $z > 3$. This indicates that the Hubble sequence is also established between these two epochs. Therefore, the most drastic evolution of galaxies such as the most active star formation, build-up of stellar mass, prominent chemical evolution, and emergence of the Hubble morphological sequence is considered to occur at the epoch of $z \sim 1 - 2$.

Mass accretion rate onto supermassive black holes also peaks at $z \sim 2$. The optical and X-ray surveys of QSOs and active galactic nuclei (AGNs) have revealed that the AGN/QSO number density and their emission density seem to be at the highest during this epoch, which means that the black hole growth rate is the highest at that time. In the present universe, the mass of the supermassive black hole residing in the center of a galaxy correlates well with the stellar-mass of the spheroidal component of its host galaxy, suggesting co-evolution of galaxy and supermassive black hole. Such a relation seems to still hold at $z \sim 1$, so the origin of the relation is expected to take place at $z > 1$.

Thus the most drastic growth of galaxies and supermassive black holes is seen at $z \sim 2$. Many of these properties have been, however, revealed in the optical band, i.e., the rest-frame UV wavelength regime. In the rest-frame UV, the effect of dust extinction is very severe and determining the true star-forming rate (SFR) and black hole accretion activity is challenging. In fact, for instance, a population of submm galaxies (SMGs) has been recently discovered at $z \sim 2$, which are probably heavily obscured massive galaxies under intense starburst with some AGN activity. The SMGs are hard to recognize at rest-UV wavelengths. In addition, there is a possibility that many highly-obscured AGNs are hidden at this epoch. Thus we have not yet determined the true star-formation and mass-accretion activities, and have not yet understood the whole population at this important epoch.

Therefore, further exploration of star formation and AGN mass accretion, and the relation between the two, is critical – particularly at the peak of such activity (the era of most violent evolution at $z \sim 1 - 2$). Such studies require us cover the

rest-frame optical regime, where the effect of dust extinction are largely mitigated, and important indicators are well-calibrated (for example to determine star-formation rates, dust extinction, gas metallicities, black hole masses, and to discriminate between AGN and star formation through emission line ratios). At $z$=1–3, the rest-frame optical light is redshifted to near-infrared (NIR) regime, and NIR spectroscopic observations are thus essential to explore this critical epoch of galaxy/AGN evolution. However, the capability of NIR multi-object spectroscopy has been very limited; although MOIRCS-type NIR multi-slit spectroscopy is available, typical multiplicities are limited to only $20 - 30$ at most, and statistical studies based on a large number of objects in the violent epoch have been very difficult.

The advent of FMOS on the Subaru Telescope will revolutionize this field with its unique and powerful characteristics. FMOS enables us for the first time to push the statistical studies of galaxy/AGN evolution into the era when the evolution is peaked, based on an unprecedentedly large sample of galaxies. Due to its outstanding multiplex capability, up to 400 objects over a very wide field of view (30 arcmin diameter) can be observed simultaneously in the NIR. Taking this unique massive advantage, we here propose to conduct a Subaru Strategic Program (SSP) with FMOS to make a comprehensive and systematic survey of galaxies and AGNs at the era of their peak evolution in the Universe, and so tackle many outstanding scientific issues in modern extragalactic astronomy.

## 1.2 Scientific objectives

Our key scientific objectives to be addressed in the proposed FMOS SSP are summarized as follows.

- Galaxy evolution
  - tracing the cosmic star-formation history with an ideal star formation indicator, H$\alpha$.
  - unveiling obscured star formation activities to obtain the true star formation history
  - understanding the origin of down-sizing (star formation history as a function of mass)
  - identifying the physical mechanisms to quench the star formation activity
  - tracking chemical evolution as an independent measure of star formation history
  - identifying the evolutionary phases of dusty star forming galaxies
  - determining the formation epoch of the oldest passive galaxies
- AGN evolution
  - revealing the presence of any heavily obscured AGN population
  - exploring the nature of mildly obscured AGNs
  - understanding the down-sizing of AGN activity
  - investigating the structure and evolution of dusty tori
  - deriving the black hole mass function and Eddington ratios
  - studying the super-Eddington accretion
- Galaxy-AGN co-evolution
  - understanding the roles of radio-mode feedback
  - identifying the conditions of AGN activation in various galaxies
  - investigating the relationship between the mass accretion rate and star-formation rate

## 1.3 Strategy

In order to achieve the above aims, we have to explore the properties of galaxies and AGNs across various parameters that govern their evolution. In this SSP, the parameters we investigate are mainly stellar mass, star-formation activity, AGN activity, level of dust obscuration, and local density (environment). Exploring these parameter spaces is indispensable to understand the whole picture of galaxy/AGN evolution. Thus combining these samples in a well-organized way within a single large program is important to achieve the scientific objectives. Traditional large spectroscopic surveys have been conducted on magnitude limited samples. However such sample can cover only a single parameter. For example, the $K$-band selected sample can probe the stellar mass parameter, while the blue/UV selected sample can probe the SFR parameter.

Although the primary parameter of evolution would be stellar mass, other parameters such as star formation activity, AGN activity (both of which are related to the feedback mechanism), the level of dust obscuration, and the local density are also crucial to understand galaxy evolution. To cover the whole range of each parameter, however, would require too large a sample of galaxies to be realistic. Therefore, we adopt the following strategy: We first set the core sample of galaxies along the stellar mass axis and star-formation activity axis. We then expand the parameter space covered using the supplementary galaxy samples to AGN activity, level of dust extinction, and local density. For this purposes, we will use: a stellar-mass and expected emission-line flux (an indicator of the apparent star-formation rate) limit; another sample of passive galaxies (with no current star-formation

Table 1. Sample summary

| Sample | Parameter space covered | Number of targets |
|---|---|---|
| core sample | stellar-mass & emission-line flux (SFR) limit | $\sim 5000$ |
| Extend-sample 1 | complete stellar-mass limit for massive galaxies | $\sim 2000$ |
| Extend-sample 2 | passive galaxies | $\lesssim 100$ |
| Extend-sample 3 | low-mass galaxies (emitters) | $\sim 5000$ |
| Extend-sample 4 | dusty star-forming galaxies (MIR/FIR/submm sources) | $\sim 2000$ |
| Extend-sample 5 | AGNs (X-ray/radio sources) | $\sim 1000$ |
| Extend-sample 6 | local density/environment (clusters) | $\sim 10$ clusters |

Table 2. Field summary

| Field | $\alpha$, $\delta$ | Nights |
|---|---|---|
| **SXDS/UDS** | 02h18m, $-05°00'$ | 53.6 |
| **COSMOS** | 10h00m, $+02°12'$ | 28.9 |
| **AKARI deep field** | 17h55m, $+66°36'$ | 6 |
| **Clusters** | see Table 4 | 20 |
| Subtotal | | 108.5 |
| **Supplementary fields** | | |
| **CDF-S** | 03h32m, $-27°48'$ | 6.6 |
| **Subaru deep field** | 13h25m, $+27°30'$ | 4.9 |
| **AEGIS** | 14h17m, $+52°30'$ | 2 |
| Subtotal | | 13.5 |
| Total | | 122 |

[1]Required nights include overhead of 40-50% and clear night fraction of 75-80%.

activity); a sample of very dusty star-forming galaxies (such as MIR/FIR/submm sources); AGNs (X-ray selected, radio selected); and clusters. These are summarized in Table 1.

The fields we employ are shown in Table 2; they are well studied regions where multiwavelength data are available. SXDS/UDS and AKARI Deep Field have been developed through extensive collaboration between UK and Japan. More details of the targets and the fields are described in §5 and Table 5.

Combining the results on all the samples together in a systematic and coherent way, within a single large program (the FMOS SSP), will be essential to provide the comprehensive studies of galaxy and AGN evolution at their peak epoch. An SSP is the most efficient way to achieve these goals. Each scientific objective is described in detail below.

## 1.4 Why SSP?

The call for Subaru Strategic Programs requires that either of the following criteria should be satisfied.
*Category A: Observations with use of an instrument having capability for large surveys, and scientific results as well as data itself are highly useful for Japanese and world astronomers. Strategic and systematic time allocation can surpass individual program allocations in terms of depth and wideness of the observations.*
*Category B: Systematic and long observations with a unique instrument are necessary to achieve important and clear science(s) beyond individual programs.*

We stress below how the proposed SSP is unique, indispensable and effective.

1. A large data set taken with unique instrument

   The proposed survey observations with FMOS well satisfy both SSP categories above. FMOS is the unique instrument among $8-10$ m class telescopes. Owing to its very high multiplicity and very wide field of view, FMOS is extremely powerful in collecting a huge number of NIR spectra of galaxies and AGNs in the violent epoch of the universe. We expect that the proposed survey will open up a new survey space for high-$z$ galaxies and thus bring us innovative scientific results. Such a large data set of NIR galaxy spectra will also be valuable for astronomers world-wide. Further, a solid understanding of galaxies in the epoch obtained through this large dataset can feedback into various computer simulations (e.g. semi-analytic modeling) to better physically motivate our modeling of of galaxy formation and evolution.

2. Well organized studies

   In order to achieve our scientific aims, we need to cover a large parameter space with respect to stellar mass, SFR, dustiness, AGN activity, and local density, etc., as already mentioned above. Various individual applications for observing a certain

target field with a various scientific aim (similar to one of ours) will be proposed with FMOS. However those individual studies may not be very efficient or systematic, as target number densities or field coverage may not fully utilize the FMOS capabilities. Moreover, depth and wavelength coverage would vary a lot among different programs which makes it difficult to compare results consistently. The proposed SSP aims to make a survey in a more systematic way and conduct the studies in a well organized way; We can share fibers among different samples within the single SSP, which will maximize the efficiency of fiber allocation. Moreover, we can make direct comparisons of the results among our samples covering a wide range of the parameter spaces mentioned above, over different cosmic epochs and across various galaxy density environments. Furthermore, such a coordinated systematic survey is ideal to study co-evolution between galaxies and AGN in the same field. These are the great advantages of applying for a large systematic survey program (this SSP), and it satisfies both category A and B. Constructing a large database of galaxies/AGNs in the violent epoch of the universe will have legacy science values not only for the Japan/UK community but also for the astrophysicists world-wide.

3. Urgency

   Although the multiplicity of FMOS is uniquely large, other telescopes with smaller multiplicity can potentially achieve these studies by a larger investment of telescope time. We (the Subaru community) therefore urge that such an SSP with FMOS is started soon, so that we can make the most of our current advantage, and be the first to cull the important science results made available by large-scale NIR spectroscopy.

4. Future studies with ALMA and others

   The FMOS SSP samples and the results from them will provide excellent inputs to future studies, especially with ALMA. The large number of spectra to be obtained with FMOS will serve as unique targets for ALMA, which is about to start science operation (in parallel to the proposed SSP). The primary aims of ALMA is to study molecular gas and dust in the violent epoch, complementing our FMOS work on stellar light and ionized gas. For example, star formation efficiency and the gas-to-star conversion factor can be examined as functions of stellar mass, SFR, and gas metallicity, etc., by coupling FMOS and ALMA data. This will give us more comprehensive, internal views of galaxy formation and evolution including the gas/dust phases of the material. The data will also surely contribute to the next generation future facilities such as thirty meter telescope, and space missions such as SPICA and JWST.

### 1.5 Note on the complementary nature to HST/WFC3

Here we highlight the complementary nature of the FMOS survey as compared with *HST*/WFC3 surveys such as 3DHST and WISP (Atek et al., 2010, ApJ 723, 104). The *HST*/WFC3 slitless mode can take NIR spectra of galaxies at the same redshift range which this SSP also targets. It reaches fainter level (e.g., a few $\times 10^{-17}$ erg s$^{-1}$ cm$^{-2}$) than FMOS (several to 10 $\times 10^{-17}$ erg s$^{-1}$ cm$^{-2}$), but in a very small FOV of a few arcmin$^2$ and at much lower spectral resolution. Even with a large survey of 3DHST, the surveyed area would be at most comparable to one FOV of FMOS. The FMOS survey covers a much wider area and should result in much better statistics especially for the relatively rare brighter/massive objects. Since the spectral resolution is $100-200$ with *HST*/WFC3 slitless mode, emission line diagnostics such as using H$\alpha$ and [NII]6548/6584 for AGN/star-forming galaxy separation and for gas metallicity cannot be used as the lines are blended. Furthermore the FMOS high resolution mode ($R \sim 2200$) can potentially probe kinematics within individual galaxies, which is impossible with the *HST*/WFC3 data.

In a part of the SXDS/UDS and the COSMOS field, *HST*/WFC3 imaging observations are being undertaken; an area of $\sim 200$ arcmin$^2$ will be surveyed in each field. These data help us to study rest-frame optical morphology and structure of the target galaxies, and our spectroscopy would greatly enrich studies with the $HST$ data.

## 2 Galaxy Evolution

A key objective in studies of galaxy formation and evolution is determining at what epoch the majority of stars formed in the Universe. Parallel to this, the metal enrichment history of galaxies provides clues to their previous star formation episodes. Charting these properties, along with the assembly of mass over a wide range of redshift and galaxy mass, allows a direct observational test of galaxy formation paradigms.

### 2.1 Star-formation activity at the violent epoch of evolution

#### 2.1.1 Tracing star-formation history with H$\alpha$ emission

Much is known about the $z < 1$ Universe from such surveys as DEEP2 on Keck/DEIMOS (Davis et al. 2003, SPIE, 4834, 161) and VVDS on VLT/VIMOS (Le Fèvre et al. 2004, A&A 428, 1043) and also star-forming galaxies at $z > 3$, now extended to redshifts as high at $z \sim 6-8$ (e.g. Bunker et al. 2004, MNRAS, 355, 374; Wilkins et al. 2010, MNRAS, 403, 938). There is much evidence to indicate that the star-formation rate in the past was much higher compared with the current epoch, perhaps by an order of magnitude at $z \sim 1$ (e.g., Lilly et al. 1996, ApJ, 406, L1). However, previous attempts to measure the global star formation history of galaxies have been flawed (e.g., Madau et al. 1996, MNRAS, 283, 1388): they have relied on different indicators of star formation in the various redshift bins, with uncertain relative calibration and are very differently affected by

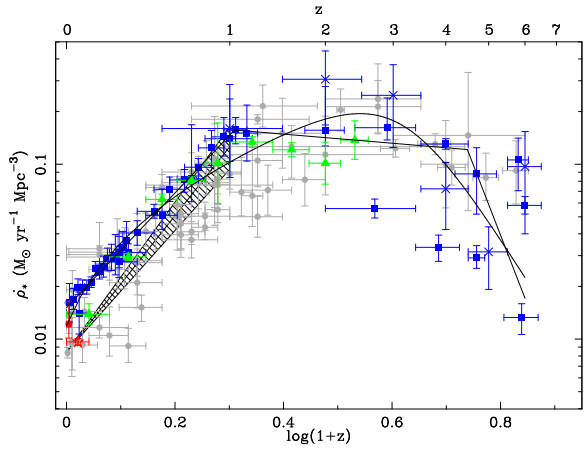


Figure 1 An updated version of the Madau-Lilly diagram, taken from Hopkins and Beacom (2006, ApJ, 651, 142). Star formation activity may peak at $z \sim 1-2$, but the data from different indicators of SFR are discrepant by an order of magnitude. A large sample of H$\alpha$ measurements at these redshifts using multi-object near-infrared spectroscopy will address this properly.

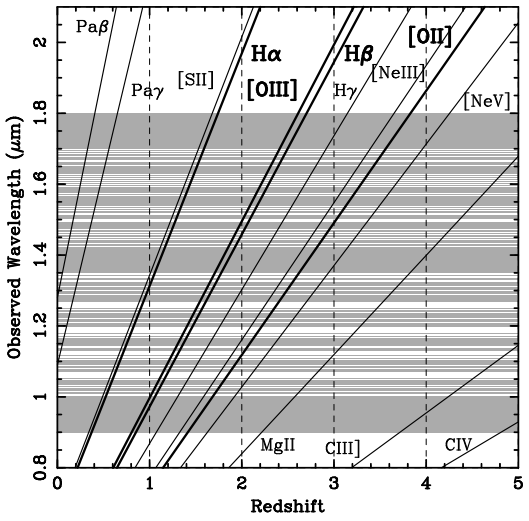


Figure 2 Observed wavelengths of major emission lines against redshift. Shaded regions show locations of OH masks and very low sensitivity region in the LR mode.

dust extinction (Fig. 1). To make a fair comparison, we need to use the same reliable instantaneous tracer of star formation at high redshift as locally. The H$\alpha$ emission line, used in surveys of star formation at low redshift, is eminently suitable as it is relatively immune to metallicity effects and is much less susceptible to extinction by dust than the rest-UV continuum and Lyman-$\alpha$ (which is also selectively quenched through resonant scattering).

However, tracing H$\alpha$ to early epochs forces a move to the near-IR at $z > 1$; the crucial epoch $z \approx 1-2.5$ where galaxy formation may peak has been relatively uncharted because of the lack of emission lines in optical spectroscopy. Building statistically significant H$\alpha$ samples at these redshifts has been difficult until now because of the inefficiency of single-object long-slit spectroscopy. Doherty et al. (2004, MNRAS, 354, L7; 2006, MNRAS,370, 331) pioneered genuine near-IR multi-object spectroscopy to survey H$\alpha$ in redshift 1 galaxies – using the MOS mode of CIRPASS instrument (the precursor to FMOS, Parry et al. 2000, SPIE, 4008, 1193) on both the AAT and WHT with 150 fibres over a $\sim$40 arcmin field. More recently, the MOIRCS instrument on Subaru (which offers multi-object near-infrared slitmask capability over a 6arcmin field) has been used to target 37 galaxies at $z \approx 2$ in GOODS-North (e.g., Yoshikawa et al. 2010, ApJ, 718, 112). Erb et al. (2006, ApJ, 647, 128) have $\approx 100$ near-infrared H$\alpha$ spectra using individual long-slit observations of $z \approx 2$ galaxies, with another 80 targeted with integral field spectroscopy (Förster-Schreiber et al. 2009, ApJ, 706, 1364). With its 400 fibres deployable over 30 arcmin, FMOS on Subaru will offer an unprecedented multiplex advantage in the near-IR – able to rapidly build up samples of many thousand galaxies, comparable to 2dF in the optical, but working at $z \sim 1$ rather than $z \sim 0.1$.

A good approach to derive the star-formation rate density with H$\alpha$ luminosity is to make use of narrow-band imaging data. HiZELS is the NIR narrow-band imaging with the aim of detecting H$\alpha$ emitters at $z = 0.84, 1.47$, and 2.23 with UKIRT/WFCAM (Geach et al. 2008, MNRAS, 388, 1473). Since the NIR narrow-band imaging can detect all the star-forming galaxies with H$\alpha$ emission above the flux limit (star-formation rate) set at the target redshift, this is a very powerful way to construct H$\alpha$ luminosity function, thus the star-formation rate density at the redshift. The resulting H$\alpha$ luminosity function at $z = 0.84$ is presented by Sobral et al. (2009, MNRAS 398, 75) (Fig 4) with a limiting H$\alpha$ luminosity of $10^{41.8}$ erg s$^{-1}$, corresponding to a star-formation rate of $\sim 5 M_\odot$ yr$^{-1}$. The value is less than $L^*$ of the luminosity function and is deep enough to probe much of the star-formation rate density at that redshift. Nevertheless there is a possibility that the sample includes contamination from lower redshift galaxies (especially Paschen emission lines) and AGNs, and the line fluxes may be underestimated if the line falls close to the wavelength edges of the narrow-band filter. In order to obtain cleaner sample of H$\alpha$ emitters, and thus more reliable star-formation rate measurements and its cosmic density, direct spectroscopic survey is essential.

### 2.1.2 Star-formation activity and stellar mass

The star-formation rate of a star-forming galaxy correlates well with its stellar mass. Daddi et al. (2007, ApJ 670, 156) clearly showed the evolution of the relation up to $z \sim 2$. This trend seems to continue to higher redshift (Gonzalez et al. 2010, ApJ, 713, 115). However there is still debate about the existence of such a clear relation, and it may have much more intrinsic scatter at higher redshift ($z \sim 2$, Yoshikawa et al. 2010, ApJ, 718, 112). Although Onodera et al. (2010, ApJ, 715, 385) claimed the relation at the same redshift is consistent with that obtained by Daddi et al. (2007), there seems to be a large scatter in this new determination. In order to investigate the relation further, in particular searching for another parameter affecting the relation, it is important to understand the star-formation history of the individual galaxies. It is also important to understand any down-sizing phenomena and the quenching mechanism of star formation in galaxies as described below.

To know what kind of galaxies mostly contribute to the star-formation activity as a function of redshift is crucial to understanding galaxy evolution across cosmic time. Recently, Gilbank et al. (2010, MNRAS, 405, 2594) showed star-formation rate density at $z \sim 0.1$ and $\sim 1$ peaks at around a stellar mass of $10^{10.5} M_{\odot}$. The rate is derived from [OII] emission line luminosity, but they pointed out the need for correction of the [OII] luminosity $-$ star-formation rate relation for massive galaxies, as the [OII] flux also on metallicity and dust extinction as well as star formation rate. With the FMOS SSP, we can derive the star-formation rates with the more reliable H$\alpha$ tracer, and also determine the metallicity and dust extinction at $z \sim 1.5$, thanks to the well organized samples (as described below), leading to a much clearer view of the stellar mass build-up process.

### 2.1.3 Obscured star formation and the true star-formation rate density

Tracing star-formation rate density with H$\alpha$ luminosity has great advantages as described above. Nevertheless, it may still miss some fraction of star-formation activity due to the dust obscuration. To obtain a better determination of the true star-formation rate, we need to reveal obscured star formation. A traditional way to derive the true star-formation rate is to determine the amount of extinction from the Balmer decrement (the ratio of H$\beta$ flux to H$\alpha$). With FMOS we can adopt this technique for galaxies at $z \sim 1.3 - 1.6$ where FMOS can cover both the emission lines.

For galaxies without measurable H$\beta$ emission, the color excess from the SED fitting can be used to estimate the obscuration. However, the effects of dust attenuation in galaxies are rather complicated, depending on the geometry of gas and stars, and also on the composition of dust. It is well known that the dust attenuation of hydrogen recombination lines from star-forming regions is systematically higher than that of the stellar continuum in galaxies (e.g. Calzetti 1997, AJ, 113, 162; Cid Fernandes et al. 2005, MNRAS, 358, 363). This differential extinction factor may become a critical source of uncertainty for deriving star-formation rates. Thus, studying the dependency of the amount of extinction against star-formation rate, stellar mass, infrared dust emission, etc., is essential to reveal the dust obscured star formation. For instance, using HiZELS Garn et al. (2010, MNRAS 402, 2017) found a trend at $z = 0.84$ that the $A_{\rm H\alpha}$ increases with increasing star-formation rate. Until FMOS, this kind of statistical study is limited mainly to local galaxies, because H$\alpha$ redshifts out of the optical window at $z \gtrsim 0.4$. This also hampers the study of the evolutionary effects of dust obscuration. We may be able to examine the evolution of such a trend and use it to correct for the extinction in galaxies at other redshifts.

However, even after correcting for the extinction by using the Balmer decrement, the true star-formation rate may be larger because of much heavier obscuration. Such heavily obscured star formation can be probed with the mid-infrared luminosity and/or the FIR/submm luminosity. In fact, evidence is mounting that (ultra-)luminous infrared galaxies are a key population in understanding the formation and evolution of galaxies. For example, more than half of the stellar mass in the local universe could be formed in galaxies with $L_{IR} > 10^{11} L_{\odot}$ (Elbaz et al. 2002, A&A, 384, 848; Wardlow et al. 2010, MNRAS in press(arXiv:1006.2137)). The cosmic star-formation rate and also the cosmic infrared luminosity density evolves as rapidly as $(1+z)^4$ up to $z \sim 1$ and luminous infrared galaxies come to dominate the cosmic star-formation activity at $z \sim 1$ (e.g. Le Floc'h et al. 2005, ApJ, 632, 169; Takeuchi et al. 2005, A&A, 440, L17; Goto et al. 2010, A&A, 514, A6). Luminous infrared galaxies at $z \sim 2 - 3$ are also often uncovered as (sub)millimeter galaxies, and these can also contribute up to $\sim 50$ % of the cosmic star-formation rate density at this (e.g., Chapman et al. 2005, ApJ, 622, 772; Hatsukade et al. 2010, MNRAS, in press).

Therefore, spectroscopic follow-up observations of luminous infrared galaxies are clearly important to know the true star-formation activity in the universe and the relation between the star-formation rate estimated from extinction-corrected H$\alpha$ and that from the mid-IR/FIR. With these data, we can evaluate the true star-formation rate and its density and the fraction contributed by these highly-obscured objects. FMOS spectroscopy is essential, since emission lines in rest-UV wavelength are expected to be extinguished heavily, while those in rest-optical wavelength are not so severe, so NIR follow-up of submm/MIR galaxies such as $AKARI$, ASTE/AzTEC, and *Herschel* sources would clarify the evolution of obscured star-formation activity, and hence the true star-formation rate and the SFR density of the Universe. One of the advantages of using FMOS is that the number densities of these sources are comparable to or slightly smaller than FMOS multiplicity in a FoV.

*AKARI*/InfraRed Camera (IRC) covers continuous wavelengths from 2 to 24 $\mu$m (Fig 3). This comprehensive wavelength coverage allows us to estimate the rest-frame 8 $\mu$m luminosity of galaxies at $0 < z < 2$ with no $k$-correction, which encompasses the important PAH 7.7 $\mu$m emission feature (frequently used as a star-formation rate indicator). Recent *Herschel* observations reveal that *Spitzer*-based star-formation rates have large uncertainties, up to a factor of 4 in the worst cases (Nordon et al. 2010, A&A, 518, L24; Rodighiero et al. 2010, A&A, 518, L25). Given good correlations between specific mid-IR emission features, such as PAHs, and total IR luminosity, a major source of uncertainty in *Spitzer*-based SFRs could be the mid-IR $k$-correction, because of the wavelength gap between IRAC 8 $\mu$m and MIPS 24 $\mu$m. The *AKARI* data are free from such uncertainty. Further, once we obtain submillimeter images from the SCUBA-2 cosmology survey or from a *Herschel*/PACS-SPIRE parallel-mode survey in the North Ecliptic Pole ($1\sigma$ = 1.6mJy at 250$\mu$m), we will incorporate the total IR luminosity in our analysis. In addition to this, with the PAH 7.7 $\mu$m luminosity we investigate how the gas metallicity regulates the dust-related properties of galaxies. We stress that it is important to understand the dependence of the rest-frame 8 $\mu$m luminosity on parameters other than star-formation rate, such as the specific star-formation rate and the gas metallicity, since this would be the only detectable dust emission in the faintest galaxies at high redshifts even with the next generation IR-submm telescopes, such as *JWST, SPICA*, and ALMA.

We can also investigate a possibility of using the the observed luminosity ratio of $L_{8\mu m}/L_{H\alpha}$ as a measure of dust attenuation in emission lines. For local galaxies, this luminosity ratio is found to correlate with the Balmer decrement (e.g. Treyer et al. 2010, ApJ, 719, 1191). We establish this correlation with the statistical sample of luminous infrared galaxies at $z \sim 1$. This correlation could be used to estimate the dust-corrected star-formation rates from H$\alpha$ for galaxies even with no H$\beta$ detection. There would

be many FMOS targets with no H$\beta$ detection, given the faintness of H$\beta$. We could apply this method for 24 $\mu$m-detected galaxies at $z \sim 2$ in the other target fields such as SXDF and SDF.

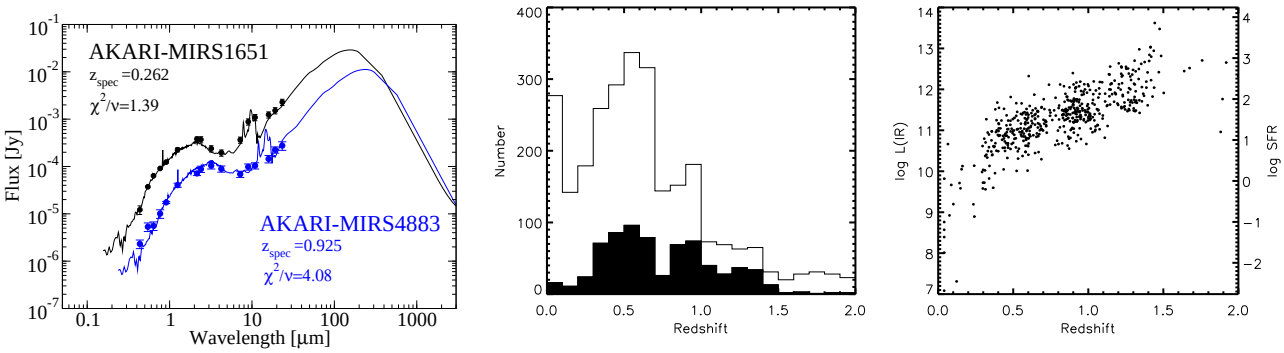


Figure 3 [Left] Example of optical-IR SEDs from the NEP-Deep survey. Although both are best-fit with the same SED template, the best-fit to MIRS4883 (blue) is rejected because the strong PAH feature in the template is not detected with *AKARI*. [Middle] Redshift distribution of mid-IR detected galaxies in the NEP-Deep (open) and FMOS targets (filled). [Right] IR luminosities and corresponding SFRs of FMOS targets as a function of redshift.

### 2.1.4 Properties of dusty star-forming galaxies

Unveiling properties of dusty star-forming galaxies is important not only to derive true star-formation rates at the violent epoch of the universe as described above, but also to understand their nature. We can perform extensive statistical studies with distant luminous infrared galaxies provided from *AKARI*, ASTE/AzTEC, and *Herschel*. With these large samples with the FMOS rest-frame optical spectra, we will be able to address the fundamental properties of these sources, i.e., (1) constraints on their redshift distributions and the volume number densities, (2) constraints on the heating source (if we detect lines such as [OIII], [NII], H$\alpha$, [OII], and H$\beta$), i.e., AGN fraction (related to §3 and §4), and (3) constraint on halo masses of them from clustering analysis using precise redshifts. For the purely starburst populations, we will also derive constraints on star-formation rate and the metallicity from these rest-frame optical lines (see §2.2 for details). If we could obtain data in clusters, environmental effects on star formation and nuclear activity could be examined as a function of the properties of the environment (related to §2.4), which will be accomplished with the largest data set with rest-frame optical spectra. Since these very dusty star-forming galaxies are expected to have large stellar masses, we may be witnessing a final large starburst phase to form the most massive class of galaxies in the present-day universe. Investigating the nature of these objects would be vital to understand the formation and evolution of massive galaxies.

Finally, it is worth stressing, especially for this population, that these studies are expected to supply very unique targets to future ALMA observations. Knowing redshifts, star-formation rates, and gas metallicity of target galaxies are indispensable to make efficient surveys of CO emission lines in these dusty star-forming galaxies. Molecular gas mass and its density/temperature as well as kinematic properties coming from ALMA will greatly help the understanding of whole picture of galaxy evolution. There is an uncertainty in the CO-to-$H_2$ conversion factor; we will study the metallicity dependence of this conversion factor. Our large sample of H$\alpha$ kinematics and metallicities is ideally suited to studying the variation in this conversion factor within metallicities and mass.

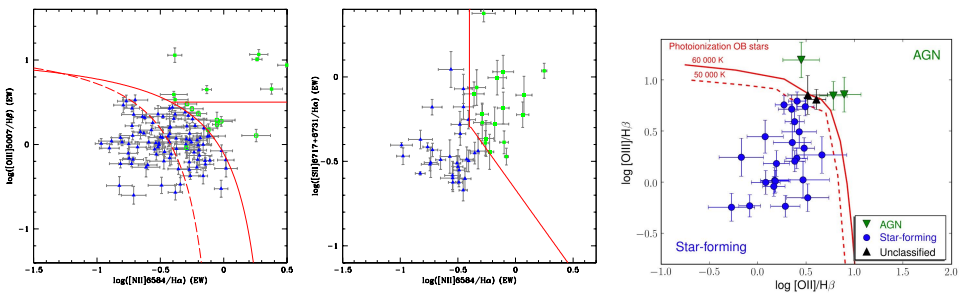


Figure 4 AGN-SF galaxy diagnostics taken from Lamareille et al. (2009) and Sobral et al. (2009). The emission lines in the diagrams are covered with FMOS at the target redshifts, and their line ratios can help the discrimination of star-forming galaxies and AGNs.

### 2.1.5 What quenches star-formation activity?

Other important aspects of exploring the star-formation activity in this epoch are to map the evolution of star formation activity in terms of the large scale structure of the universe and to explore the quenching of star-formation activity. Recent study by Peng et al. (2010, ApJ, 721, 193) based on SDSS and zCOSMOS data showed the following simple relations in galaxy properties at $z \lesssim 1$ : (i) the star-formation rate of star-forming galaxies scales almost linearly with stellar mass, and is independent of environment (local galaxy overdensity) at $z \simeq 0$. This relation still holds up to $z \simeq 2$ by increasing the normalization (e.g., Daddi et al. 2007, ApJ, 670, 156), with the normalization tending towards a constant value at higher redshifts ($z \gtrsim 3$, Gonzalez et al. 2010, ApJ, 713, 115); (ii) Up to $z \simeq 1$, the fraction of quenched galaxies increases steadily both with galaxy mass and local overdensity, so two distinct processes must be responsible for quenching star formation in galaxies, one related to environment and the other related to mass, and thus the effects of mass and environment in quenching of galaxies are separable. Based on these observational relations and a postulation that these hold beyond $z \simeq 1$, Peng et al. (2010) demonstrate that the shape (i.e, a double Schechter function) and evolution of the mass function for all galaxies, including those that have had their star formation quenched, are a natural consequence of these fundamental relations.

One obvious question is whether this empirical evidence holds at $z \gtrsim 1$. While such evidence exists beyond $z \gtrsim 1$ for the relation between star-formation rate and stellar mass, the separability of two quenching processes remains to be confirmed. To answer to this question, one needs to properly locate many galaxies in the large scale structure and compare galaxy properties at these redshifts with environment. However, at $z > 1$, in particular at $1.4 \lesssim z \lesssim 2.5$ , spectroscopic identification has been quite difficult because of no strong spectral feature in the optical. Even one of the best-efforts to date, zCOSMOS-deep (Lilly et al. 2007, ApJS, 172, 86; Lilly et al. 2009, ApJS, 184, 218) which has identified $\simeq 5000$ star-forming galaxies at $1 < z < 3$, has been hampered by the limit of $B_{\rm AB} = 25$.

To remedy the shortcomings of current surveys, FMOS is an ideal instrument to study star-forming galaxies over wide area in the redshift desert since one can detect bright emission lines such as [OII] and H$\alpha$ shifted into the NIR (Fig 2) with enormous multiplicity, which is necessary to map the large scale distribution of galaxies in the field. With FMOS redshifts combined with currently-available spectroscopic redshifts, we will be able to identify large scale structures from field to group/cluster environments at $z > 1$ and relate them with galaxy properties such as mass, star-formation rate, metallicity (§2.2), AGN activity (§3) and morphology. However, the densest environment of the Universe (rich clusters) would not be covered in the general field survey. Therefore the sample of selected clusters as proposed in § 2.4 will complement such environmental studies in particular in cluster cores and in groups in the vicinity of rich clusters.

### 2.1.6 Ages of passive galaxies

Quenching star formation in a fraction of massive galaxies could occur in the earlier epoch than our target redshift. Studying passively evolving galaxies at $z > 1.4$ is very important to constrain the period from the last major star formation, i.e., formation epoch of early-type galaxies such as elliptical galaxies in the present epoch, which may connect to the starburst activity seen in submm galaxies. In the local universe, early-type galaxies and bulges include almost 60% of the total stellar mass, and therefore the formation and evolution of this galaxy population are central to the broader problem of galaxy evolution in general. Among the currently available redshift surveys targeting $z > 1$ galaxies, however, passive galaxies have been virtually ignored except for a few cases (e.g. Cimatti et al. 2008, A&A, 482, 21), because their extremely faint rest-frame UV continuum requires extremely long integration $\gtrsim 30$ hours in case of Cimatti et al. (2008).

The strongest spectral features to determine the redshift of a passive galaxy are Ca II H&K and 4000Å break, but by $z = 1.4$ these features move to the NIR. So to effectively identify the galaxy population at $z > 1.4$, observations in the NIR are essential. Recent observations show that it is feasible to identify passive galaxies at $z > 1.4$ with 8–10m class telescopes (e.g., Kriek et al. 2008, ApJ, 682, 896; Onodera et al. 2010, ApJ, 715, L6). Further, Onodera et al. (2010) detected absorption lines in rest-frame optical from a passive BzK galaxy at $z = 1.82$, and constrained the age of the stellar population by using full spectroscopic information taken with Subaru/MOIRCS. Previous NIR spectroscopic observations of high-$z$ passive galaxies, however, still suffer from relatively small FoV and multiplex of MOIRCS and the inefficiency of single slit instruments.

With FMOS, we expect we will be able to detect the 4000Å break and/or rest-frame optical absorption lines of bright passive galaxies at $z > 1.4$, which constrain the ages of them from spectral fitting with stellar synthesis model. Candidate passive galaxies can be selected by BzK technique (pBzKs) combined with non-detection in infrared bands, e.g., *Spitzer*/MIPS 24$\mu$m, to eliminate a small contamination of dusty star-forming galaxies. Thanks to the wide FoV of FMOS, we can select reasonable numbers of passive galaxies.

## 2.2 Metallicity of star-forming galaxies at $z \sim 0.7 - 2.4$

Gas metallicity is a key parameter for knowing the stage of galaxy evolution because it reflects a result of past star-forming activity in a galaxy. It is also related to the history of gas inflow/accretion into and outflow from a galaxy. Thus the gas metallicity constrains the formation and evolution processes of a galaxy, and hence measuring gas metallicity of star-forming galaxies in the drastic evolution phase is imperative to understand galaxy evolution. For example, based on metallicity measurements at $z \sim 2$, Erb et al. (2006, ApJ, 644, 813) and Erb (2008, ApJ 674, 151) argue that gas inflow is required to sustain a high star-formation rate and that gas outflow comparable to the star-formation rate can reproduce the mass-metallicity relation at $z \sim 2$ (right most panel of Fig 5); a similar conclusion is obtained from simulations by Finlator and Dave (2008, MN 385, 2181). The

metallicity study also sheds light on chemical evolution of the intergalactic matter. Further, by estimating the effective yield from the metallicity and gas-mass fraction, we may be able to obtain a clue as to the initial mass function.

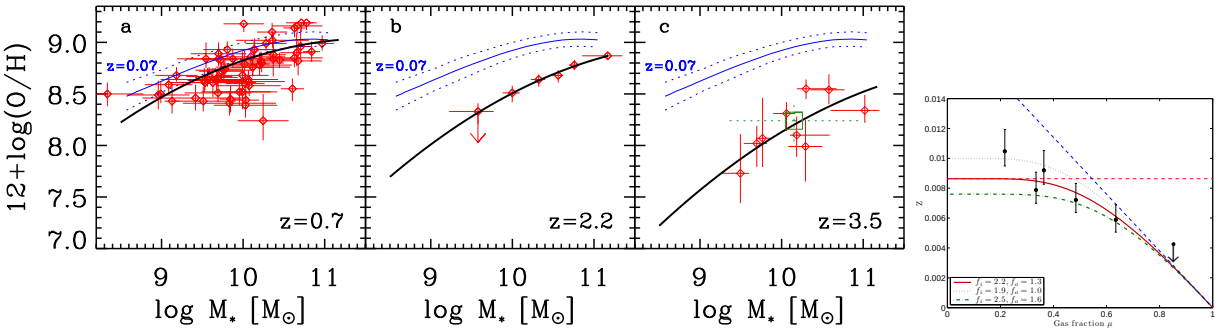


Figure 5 Left:Mass-metallicity relations at $z = 0.07$(Tremonti et al. 2004), 0.7 (Savaglio et al. 2005), 2.2 (Erb et al. 2006), and 3.5 (Maiolino et al. 2008) from Maiolino et al. (2008). FMOS will show the relation at $z \sim 1-2$, not only against stellar mass, but also against another parameter such as star-formation rate etc. thanks to its large sample. Right: metallicity vs gas mass fraction from Erb (2008). Model curves show comparable amount of inflow and outflow is needed to reproduce the observed values. With more data points with smaller error bars, the gas infall/outflow process will be well constrained.

The presence of a stellar mass-metallicity relation is well established at $z \sim 0.1$ (e.g., Tremonti et al. 2004, ApJ, 613, 898, $z = 0.07$ in Fig 5); massive galaxies show higher gas metallicity indicating more chemical evolution than lower-mass galaxies. Savaglio et al. (2005, ApJ, 635, 250) showed an evolution of the stellar mass-metallicity relation at $z = 0.7$ such that in the massive part ($> 10^{10} M_{\odot}$), metallicity is almost the same as that at $z \sim 0.1$ while in the less massive range metallicity is less than that at $z \sim 0.1$ by $0.2-0.3$ dex on average at a fixed stellar mass, suggesting a down-sizing nature for metallicity evolution (Fig. 5 left). At higher redshifts, Erb et al. (2006) found a mass-metallicity relation of star-forming galaxies at $z \sim 2.2$ that shifts downward by 0.56 dex from the $z \sim 0.1$ relation (Fig. 5 middle). They also showed that the amount of the shift is smaller in the massive part than that in the less massive part, again suggesting the down-sizing nature of the metallicity evolution. Maiolino et al. (2008, A&A, 488, 463) studied the mass-metallicity relation of star-forming galaxies at $z \sim 3.5$ and found a further downward shift of the relation (Fig. 5 right). However, this evolution of the mass-metallicity relation is still not reproduced with most of simulations (Maiolino et al. 2008); simulations including feedback mechanism show higher metallicity than that observed at $z \sim 3$.

More recent observations, however, show a contradictory picture. Lamareille et al. (2009, A&A, 495, 53) and Pêrez-Montero et al. (2009, A&A, 495, 73) obtained a mass-metallicity relation at $z = 0.2-0.9$ and at $z = 0.9-1.24$, respectively, and found that the downshift is smaller in the lower mass range suggesting an anti-downsizing nature of evolution, though the scatter is large at a fixed stellar mass. They suggest an open-box model for lower mass galaxies (with gas outflow), while a closed-box model is proposed for massive galaxies. Further, Hayashi et al. (2009, ApJ, 691, 140), Onodera et al. (2010, ApJ, 715, 385), and Yoshikawa et al. (2010, ApJ, 718, 112) examined gas metallicity of star-forming galaxies at $z \sim 2$ and found a mass-metallicity relation that does not agree with that of Erb et al. (2006). Although the cause for the discrepancy is not clear, one possible reason for this is the sample selection; Erb et al. used UV-selected BM/BX galaxies (Maiolino's sample is also UV-selected), while the more recent studies are based on K-band selected sBzKs and include redder galaxies. BM/BX galaxies locate in a very blue region in the BzK plane (Grazian et al. 2007, A&A, 465, 393), and their evolutional stage may be different (metallicity calibration is not a main cause, because they use the same method for deriving gas metallicity).

Clearly further investigations of the gas metallicity are necessary. We have to examine the dependence of gas metallicity not only on stellar mass, but also on various parameters such as age, color (e.g., location on BzK plane), star-formation rate, specific star-formation rate, color excess (extinction), environment (local density), etc. In fact, Sol Alonso et al. (2010, A&A, 514, A57) pointed out that galaxy interactions may cause the scatter in the mass-metallicity relation using data from the SDSS and MGC. With SDSS data, Mannucci et al. (2010, MNRAS 408, 2115) claimed that star-formation rate is another parameter related to the gas metallicity. However, studying such dependence at high redshifts is a hard task, because we need to have a much larger sample to divide into many parameter bins. A typical sample size of the previous studies at $z \sim 2-3$ is only a dozen, except for the sample by Erb et al. (2006) ($\sim 90$ galaxies). This is because of a lack of multiplex capability in NIR spectroscopy; a typical NIR MOS (e.g., Subaru MOIRCS) can cover 20-30 targets in its field of view. FMOS can take up to 400 spectra simultaneously from $\sim 1.0\mu$m to $\sim 1.7\mu$m. Thus with FMOS, we will be able to obtain unprecedentedly large numbers of NIR spectra of star-forming galaxies.

To derive the gas metallicity with FMOS, there are a few appropriate methods (depending on redshift): the R23 method using H$\beta$, [OII]3727, and [OIII]4959/5007 for $z \sim 1.7-2.4$; the N2 method using H$\alpha$ and [NII]6584 for $z \sim 0.7-1.6$; and the O3N2 method using H$\beta$ and [OIII]5007, in addition to N2 method for $z \sim 1.3-1.6$. The O3N2 method has an advantage in measuring metallicities larger than about solar metallicity. Here we note that the resolution of FMOS low-resolution mode is good enough to separate the H$\alpha$ and [NII] lines; Fig 6 shows an H$\alpha$ emission line with $2 \times 10^{-16}$ erg s$^{-1}$ cm$^{-2}$ obtained with 2-h exposure time, indicating we can achieve reasonable separation of the lines. If the [NeIII] method is adopted (Nagao et al. 2006, A&A,

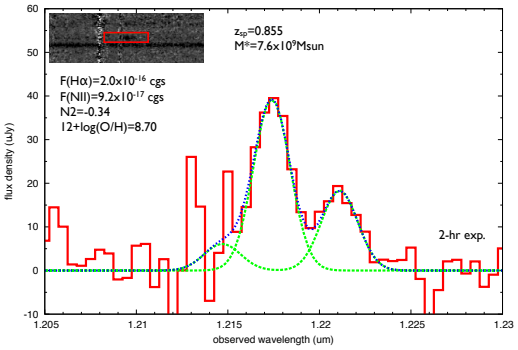


Figure 6 H$\alpha$ and [NII] emission taken with FMOS with a 2-hour exposure time together with a result of line fitting. It shows H$\alpha$ and [NII] emission lines can be clearly separated even with low resolution mode.

459, 85), we can extend the target redshift up to $z \sim 3.4$, because this method uses only the emission lines of [OII]3727 and [NeIII]3869. The accuracy of the [NeIII] method is improved with Balmer lines (Pêrez-Montero et al. 2009).

## 2.3 Probing the building blocks of present-day galaxies:low-mass galaxies at the epoch of violent evolution

In current hierarchical models of galaxy formation, small galaxies form first and then merge to produce larger systems. On the other hand, a number of observations support 'down-sizing' picture (e.g., Cowie et al., 1996, AJ, 112, 839; Kodama et al., 2004, MNRAS, 350, 1005; Bundy et al. 2006, ApJ 651, 120); more massive galaxies have completed their major star-formation than less massive galaxies. In order to test these competing scenarios, it is essential to investigate not only massive galaxies such as those found by photo-$z$ technique, but also less massive galaxies that play a major role in galaxy formation under the hierarchical framework. Moreover, less massive galaxies hold the key to understanding galaxy formation and evolution, because the evolution of mass-metallicity relation indicates that less massive galaxies show a larger decrease of metallicity from low-$z$ to $z \sim 3$ (Maiolino et al., 2008), though more recent results do not necessarily show this trend (§2.2). Since less massive galaxies at $z \sim 2$ have higher specific star formation rates, less massive galaxies intensively increase their mass during a short period of time at this epoch (Reddy et al., 2006, ApJ, 644, 792; Erb et al., 2006, ApJ, 647, 128). Thus, the important epoch for studying less-massive galaxy studies is $z \sim 2$.

One effective method to select less massive galaxies is to identify emission line galaxies, or emitters, by narrow-band imaging. Since the pioneering emission-line surveys (e.g., Smith 1975, ApJ, 202, 591;MacAlpine et al. 1977, ApJS, 34, 95), this selection method has been shown been extremely effective at detecting intrinsically faint galaxies, has been helping to overcome the biases imposed by magnitude-limited selection. Furthermore, emitters are selected on the presence of strong lines and so are easy to spectroscopically identify. Spectra of emitters can be studied on an individual galaxy basis, and can also be stacked to investigate the average properties of faint emitters that are far below the detection limits of 8m-class telescopes.

We will uncover a low-mass population of galaxies at $z \sim 1-2$ by FMOS spectroscopy, and characterize roles of these low-mass galaxies in the galaxy formation history. We will investigate 1) star-formation activities (reliably corrected for dust extinction if H$\beta$ is detected), 2) metal abundance of the inter-stellar medium, and 3) galaxy inflow/outflow and dynamical mass constrained from line widths for our emission line galaxies with a stellar mass of $\lesssim 10^9 M_\odot$ (with FMOS high resolution mode), which will complement massive-galaxy studies from our other FMOS observations as well as the previous Keck and VLT surveys (Erb et al., 2006; Maiolino et al., 2008). Because strong emission line objects include metal-poor young starbursts, we can extend our probe to a parameter space close to that of primordial galaxies.

## 2.4 Transformation of galaxies in dense environment during cluster formation

The aim here is to extend the parameter space of galaxy evolution studies to another key axis, that is "environment". The general field surveys proposed so far would tend to undersample rich, dense environments of the Universe like clusters of galaxies and their immediate neighboring regions, in particular the systems with masses greater than $10^{15} M_\odot$, even in a wide-field survey over a square degree or so. Therefore we propose here to make systematic targeted observations on $\sim$10 selected well-studied high-density regions at various redshifts ($0.55 < z < 3.1$) spanning over the epoch of violent evolution of galaxies in the Universe. By mapping out star-formation activities as functions of environment, time, and mass, we aim to identify physical processes that drive the environment-dependent galaxy and AGN formation and evolution.

It is well known that properties of galaxies such as morphology and spectral type depend strongly on environment in the sense that E/S0 galaxies with old stellar populations preferentially reside in dense environment, while spiral galaxies with active star formation are located in lower density environment. This indicates that galaxy formation and subsequent evolution is closely related to the surrounding environments. There seem to be two types of effects behind it: (I) Intrinsic ("nature") effect called "biased galaxy formation" where higher density regions collapse earlier and galaxy formation is more accelerated, whereas

lower density regions collapse later and galaxies formation is delayed (Cen & Ostriker 1993, ApJ, 417, 415); and (II) External ("nurture") environmental effects such as galaxy-galaxy interactions and ram-pressure gas stripping which influence galaxy types and star forming activities as they assemble to higher density regions (Moore et al. 1996, Nature, 379, 613; Abadi et al 1999, MNRAS, 308, 947). Although identifying the origin of environmental variation is of fundamental importance, the relative importance of these two types of effects has remained elusive.

To resolve this situation, we should (a) study galaxies higher redshifts to see the intrinsic effect as the galaxy formation bias becomes stronger in the past, and (b) go further out from the cluster core so that we can cover the infall region to witness any external effects in action directly as seen at low redshift by Lewis et al. (2002, MNRAS 334, 673). Tanaka et al. (2005, MNRAS 362, 268) found for the first time that the colour distribution of galaxies changes sharply redwards in medium density regions (groups or cluster outskirts) rather than in dense cluster cores for all clusters studied at $z \lesssim 0.8$. This indicates the importance of such environments as the possible sites of the external effects. Further, the narrow-band surveys of [OII] (RXJ1716 at $z = 0.81$ and XCS2215 at $z = 2.46$) and H$\alpha$ emitters (RXJ1716), with Suprime-Cam and MOIRCS, respectively, have also been performed reaching down to a dust-uncorrected star-formation rate of 1.5 and 3 $M_{\odot}$ yr$^{-1}$, respectively. ¿From these unique data, it is found that H$\alpha$ emitter candidates in RXJ1716 avoid the cluster center (<200kpc) and are preferentially located in the outlying regions of the cluster (Fig 7 left), suggesting that the star-formation activity has already finished in the cluster core but is probably enhanced in the medium density regions (Koyama et al. 2010, MNRAS, 403, 1611). This interesting result is also reproduced by *AKARI* 15$\mu$m imaging of this clusters, which captures strong PAH features from the cluster and is sensitive to dusty star formation. *AKARI* sources also avoid the cluster core and many are located in the surrounding region or in groups (Koyama et al. 2008, MNRAS, 391, 1758). In contrast, [OII] emitter candidates in the higher redshift cluster XCS2215 are seen all the way in to the cluster centre (Fig 7 right), suggesting high star-forming activity even in the cluster core (Hayashi et al. 2010, MNRAS, 402, 1980), although AGN contamination may be an issue especially in the red galaxies (Yan et al. 2006, ApJ, 648, 281). This may indicate an inside-out propagation of star formation activity in clusters between these two epochs (Hayashi et al. 2010).

Such an impressive difference in the spatial distribution of star-formation activity between these two clusters may indicate that the galaxy formation bias is getting more effective and visible in high density regions at $z\sim$1.5. We may be looking at the epoch when such bias starts to reverse the well-known lower-$z$ relationship of decreasing star-formation activity with increasing density. It seems that the star-formation activity is once very high in the cluster core at $z\sim$1.5, but is truncated from the center and propagated to outer regions with time (Fig 8).

Although all the results presented above, based primarily on imaging observations (broad- and narrow-band), are all intriguing, we need to investigate them in much greater detail and precision with spectroscopy, and also systematically, over a large sample of clusters. Mapping the star-formation activity directly and accurately out to large distances from the cluster centres and at various redshifts is the basic, and yet essential approach required in order to identify the physical mechanisms that determine the environmental variation in galaxy evolution.

Can we identify the epoch and the site of environmental transformation of galaxies seen as starbursts and/or truncation? For this purpose, H$\alpha$ is the best indicator of on-going star formation activity. FMOS will revolutionize the current situation and will make a break-through in this area due to its large grasp for H$\alpha$ surveys at high redshifts with 400 simultaneous targets over a 30$'$ field. Also, by applying the Balmer-decrement technique, we can make precise corrections for dust extinction. Moreover, the line ratio between H$\alpha$ and [NII] measures gaseous metallicity in HII regions, which provides independent information on the (cumulative) star-formation history. Furthermore, by combining the emission lines, we can separate out AGNs and star formation and trace their co-distribution within the large-scale structures. The environmental dependence of AGN activity, if any, along with that of host galaxies, will give us a clue to understanding the physical processes of external effects and eventually the AGN-starburst-spheroid connection (§4 for more details).

Considering these unique advantages of FMOS, we propose to include in this SSP, systematic NIR spectroscopic survey of high-density regions at $z = 0.6 - 3.1$, for which we have extensive data sets of wide-field imaging and optical spectroscopy and have already identified prominent large scale structures in and around the clusters. Our immediate scientific objectives are: **(1)** To probe kinematical sub-structures in and around the clusters based on 400–800 redshifts per cluster to see the hierarchical growth of clusters directly. **(2)** To measure accurate star-formation rates with H$\alpha$ and Balmer decrement (H$\alpha$/H$\beta$ where available). We will compare them as functions of environment and redshift to identify the site and the epoch of enhancement and/or truncation in star formation activity. **(3)** To measure metallicities of the ionized gas in star forming galaxies using either the [NII]/H$\alpha$ ratio or the oxygen based indicator R23. By comparing metallicities as functions of redshift, environment, and mass of galaxies, we will address star-formation histories on this cumulative measure "independently" from the direct measure of star-formation rates from H$\alpha$ and [OII]. **(4)** To identify AGNs using line ratios (where available) and compare their environmental variation with that of host galaxies to investigate the AGN-starburst-spheroid connection. **(5)** To try to measure Balmer absorption lines (H$\beta$) in co-added spectra of "red" galaxies especially in group environment to see any sign of post-starburst signature (e.g. Tanaka et al. 2006). **(6)** To compare these results with those obtained in the general fields to examine the effect of environment. **(7)** To compare the observational results in the general fields and in the higher density regions with the GALFORM semianalytic model and the Millennium simulation both available through this Japan-UK collaboration to understand physics behind the observed phenomena.

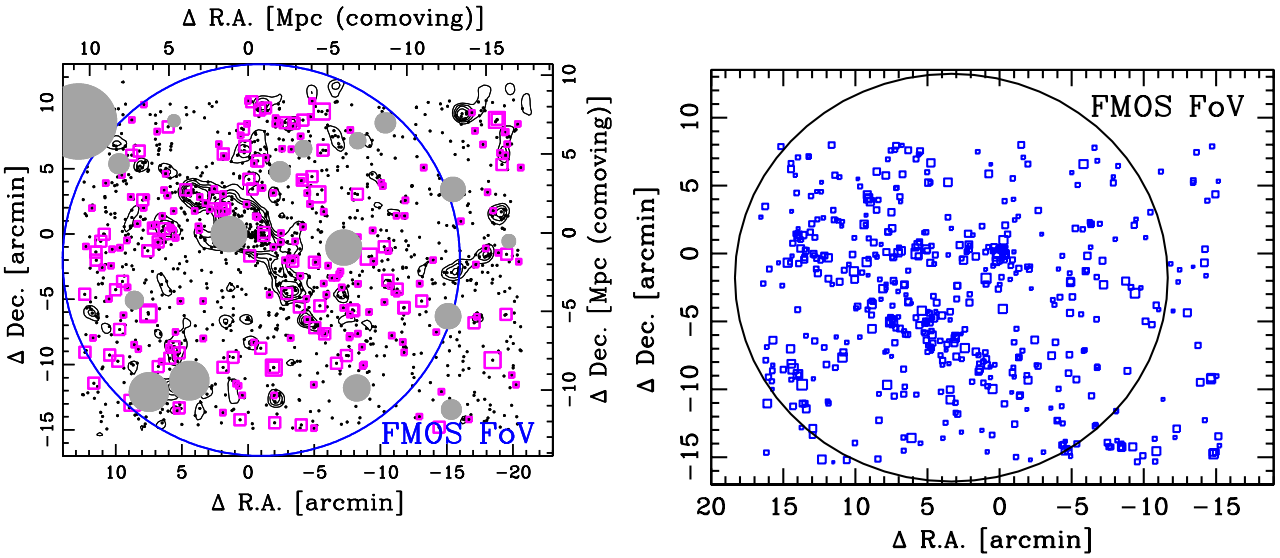


Figure 7 (left): A 2-D map of RXJ1716 cluster ($z$=0.81) (Koyama, et al., 2010, MNRAS, 403, 1611). Open squares show [OII] emitter candidates associated to the cluster selected by our narrow-band (NA671) imaging with Suprime-Cam. The size of the symbol denote the line flux. The other small dots show the phot-$z$ selected member galaxy candidates. A large circle indicate the FoV of FMOS and most of the structures and the [OII] emitters are covered by the single pointing. We will take two fibre configurations to maximize fibre allocation to the targets in the crowded regions. (right): A 2-D map of XCS2215 cluster ($z$=1.46) (Hayashi, et al., 2010, MNRAS, 402, 1980). Open squares show [OII] emitter candidates associated to the cluster selected by our narrow-band (NB912) imaging with Suprime-Cam. We will also take two fibre configurations on the single pointing as indicated by a large circle.

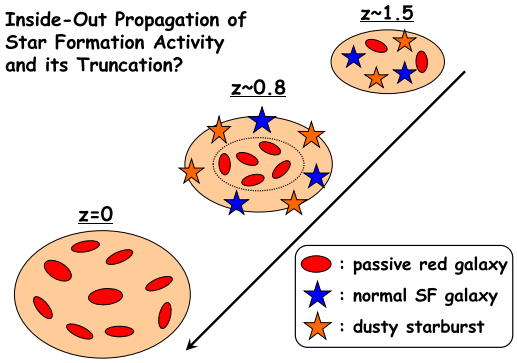


Figure 8 A schematic diagram showing our working hypothesis of inside-out propagation of star formation activity with time suggested from our wide-field narrow-band emitter surveys.

## 3 AGN populations and their evolution

With the discovery of a supermassive black holes (SMBH) at the center of every massive galaxy, the issue of how these SMBHs formed and evolved over time has become one of the major unanswered questions in modern astronomy. The total mass in present-day SMBHs is roughly consistent with the observed AGN accretion activity, which therefore implies that the main epoch of SMBH growth was during the violent era of the universe at $z$ ∼1–2.5. However, our understanding is not yet complete due to the existence of a large number of obscured AGNs which are easily missed in current surveys that rely on optical spectroscopic follow-up. NIR spectroscopy with FMOS is able to reveal the obscured accretion with observations of hard X-ray-selected AGNs and massive galaxies and determine the contribution from this elusive population.

A further key constraint on SMBH evolution comes from the evolution of the black hole mass function, which can be derived from observations of broad-line AGNs. However, current observations cannot differentiate between models because they do not sample sufficiently low masses (below the 'knee' of the mass function) at the epoch of rapid growth. FMOS provides the opportunity to remedy this by making observations of H$\beta$ in broad-line AGNs which provide reliable estimates of the black hole

mass.

## 3.1 Obscured growth of super-massive black hole during the violent epoch

The growth history of SMBHs by accretion is directly related to the evolution of the space density of AGNs. Hard X-ray surveys provide the most efficient and cleanest sample of AGNs, and intensive optical spectroscopic follow-up of sources from these surveys has revealed broad-line (type 1) and narrow-line (type 2) AGNs out to $z \sim 5$. Surveys with a range of X-ray depths have been used to calculate the number density of unobscured and mildly-obscured AGNs as a function of redshift and luminosity (e.g., Ueda et al. 2003, ApJ, 598, 886, as shown in the left panel of Fig. 9). These data have allowed the mean growth history of SMBHs to be quantitatively inferred (e.g., Marconi et al. 2004, MNRAS, 351, 169): massive ($> 10^8 M_\odot$) SMBHs grow most rapidly at $z \sim 2$ while less-massive ($< 10^8 M_\odot$) SMBHs increase their mass at $z \sim 1$. The peak epochs of SMBH growth and violent galaxy evolution are therefore concurrent.

However, a large number of obscured AGNs are missed by the current optical spectroscopic follow-up of X-ray sources (Fig. 10). We will use FMOS to overcome the current limits of out understanding of obscured accretion by (1) NIR spectroscopic follow-up of optically-faint X-ray sources, and (2) NIR spectroscopic survey of stellar mass limit sample of massive galaxies with photometric redshifts to search for AGN emission lines.

The sample of obscured AGNs is also important to understand the co-evolution of galaxies and AGNs, because detailed properties of AGN host galaxies can be examined for the obscured AGNs. Using stellar mass and age estimated from SED fitting with spectroscopic redshift, AGN host galaxies can be located among non-AGN galaxies, and the effect of AGN to the galaxy evolution can be discussed.

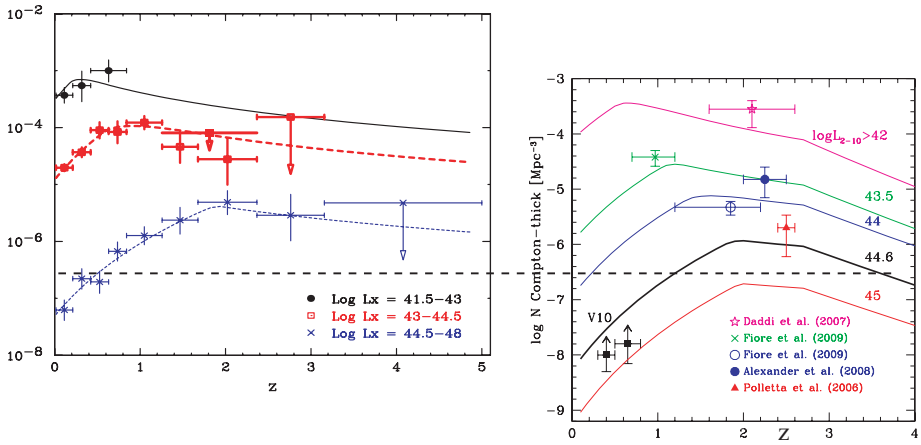


Figure 9 Number densities of non-Compton-thick (left; X-ray selected from Ueda et al. 2003) and Compton-thick (right; from Vignali et al. 2010) AGNs are compared as a function of redshift and luminosity. The estimated number density of Compton-thick AGNs are based on candidates of Compton-thick AGNs from various methods and the solid lines in the right panel are the number density of Compton-thick AGNs predicted by Gilli et al.'s (2007) model. Although the model predicts similar number density to non-Compton-thick AGNs, the observational constraints on the number density is not conclusive due to small size of each sample and complicated selection method. Rest-frame optical emission line survey of massive galaxies with FMOS will provide more systematic estimate on the number density of Compton-thick AGNs. The dashed line represent survey volume of the SXDS.

### 3.1.1 Mildly-obscured accretion revealed by an X-ray AGN survey

A significant fraction of the sources in deep X-ray surveys remain unidentified even after intensive spectroscopic observations, due to the faintness of their optical counterparts. As shown in Fig. 10, optical spectroscopic observations can reveal the nature of X-ray sources brighter than $i$ ∼23.5 mag, but many sources have fainter optical counterparts. Photometric redshift estimation suggests that the optically-faint spectroscopically unidentified X-ray sources are located at $z > 1$ (see right panel of Fig. 10). Redshift determination is made difficult not just by the optical faintness, but also because no strong AGN emission lines are visible at optical wavelengths in the range $1.3 < z < 2.3$. The best estimates suggest that obscured AGNs outnumber unobscured AGNs in the redshift range $1 - 3$, and that the obscured fraction of X-ray-selected AGNs at $z > 2$ may be twice as high as in the local universe (Hasinger et al. 2008, A&A, 905, 922).

In order to constrain the number density of mildly-obscured AGNs, we will conduct FMOS spectroscopic observations of optically-unidentified X-ray sources in the wide and deep X-ray survey regions, SXDS/UDS and COSMOS, (and supplementary CDFS). For example, among 900 X-ray sources in the SXDS/UDS region, there are 500 X-ray sources which do not have spectroscopic redshift information. Although we have photometric redshifts for the targets, spectroscopic redshift information is necessary to disclose the nature of optically-faint X-ray sources. The spectroscopic redshift information is also important to understand the photometric properties of host galaxies of obscured AGNs through SED fittings.

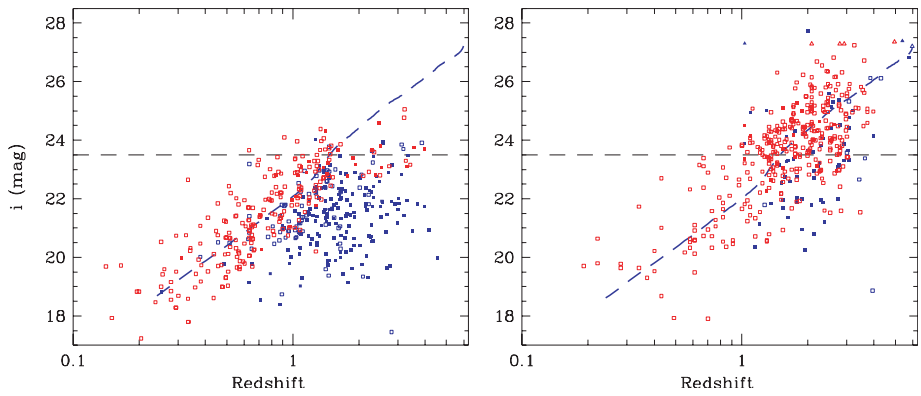


Figure 10 $i$-band magnitude against redshift of X-ray selected objects in the SXDS field. The left panel shows objects with spectroscopic redshifts, while the right panel shows the photometric redshifts of objects without spectroscopic IDs. Blue and red symbols show broad-line and narrow-line AGNs, respectively (separated by best-fit SED in the right panel). Photometric redshift estimation suggests that in the peak epoch there are large number of obscured AGNs which are missed in the optical spectroscopic sample. FMOS NIR spectroscopic survey for such optically-faint sources is crucial to disclose the nature of the sources.

### 3.1.2 Heavily-obscured accretion revealed by a Compton-thick AGN survey

Although X-ray selection is efficient for selecting mildly-obscured AGNs, it can miss and therefore be biased against heavily-obscured AGNs with column densities $N_{\rm H} > 10^{24}\,{\rm cm}^{-2}$. In these Compton-thick AGNs, where the optical depth for Compton-scattering of X-ray photons is larger than one, even the very hard (20–40 keV) X-ray flux can be diminished significantly, and samples selected in X-ray are biased against Compton-thick AGNs (Malizia et al. 2009, MNRAS, 399, 944).

In the local universe, a significant fraction of [OIII]-line-selected type-2 AGNs in the SDSS may be Compton-thick, as approximately half of them have X-ray fluxes significantly smaller than predicted from their [OIII] line luminosities (see Fig. 11, Vignali et al. 2010, MNRAS, 404, 48). The large $L_{\rm [OIII]}$ / $L_{2-10{\rm keV}}$ ratios imply that their active nuclei are heavily-obscured, even in the hard X-ray band.

Because the integrated X-ray emission from galaxies detected in current X-ray surveys cannot explain the energy density of the Cosmic X-ray Background (CXB) at its peak energy (∼30 keV), it is believed that Compton-thick AGNs must exist in large numbers, with a number density as high as that of mildly-obscured AGNs (Ueda et al. 2003; Gilli et al. 2007, A&A, 463, 79). The estimated number density of Compton-thick AGNs is summarized in the right panel of Fig. 9, and comparison with that of X-ray-selected AGNs (left panel) suggests that Compton-thick AGNs are as numerous as unobscured and mildly-obscured AGNs, and therefore must contribute significantly to the accretion growth of SMBHs. A high number density of Compton-thick AGNs at high redshift has also been inferred from AGN samples selected by 24-$\mu$m excess (Daddi et al. 2007, ApJ, 670, 173; Fiore et al. 2008, ApJ, 672, 94; Alexander et al. 2008, AJ, 135, 1968), mid-IR plus radio emission (Martínez-Sansigre et al. 2007, MNRAS, 379, L6), and MIR-SED analysis (Polletta et al. 2006, ApJ, 642, 673). However, our current knowledge on the number density of obscured AGNs is rather heterogeneous and uncertain. The redshift range our FMOS survey will probe is especially important because the residual CXB spectrum implies that the contribution from heavily-obscured AGNs peaks at $z \sim 1.5$ (Worsley et al. 2005, MNRAS, 357, 1281).

In this SSP, selected by photometric redshift and estimated stellar mass, can constrain the number density of heavily-obscured AGNs in the same way as the [OIII] emission-line survey of SDSS. Because almost all X-ray-selected AGNs are associated with relatively massive galaxies ($M_* > 10^{10.5} M_\odot$; Yamada et al. 2009, ApJ, 699, 1354), heavily-obscured AGNs are expected to also reside in such massive galaxies. Furthermore, there are suggestions that the AGN fraction among massive galaxies may be rather higher in the distant universe; a NIR survey of 26 $K$-bright galaxies at $2.0 < z_{\rm phot} < 2.7$ by Kriek et al. (2007, ApJ, 669, 776) found 11 emission line objects, including 4 classical AGNs and 3 possible AGNs (AGN+Starburst), but only 1 of these 7 objects is detected in X-rays. This implies that a significant fraction (∼1/3) of massive galaxies show AGN activity detectable with rest-frame optical spectroscopy, but most of them will be missed in deep X-ray surveys. While the size of this sample is too small to draw a firm conclusion about the number of heavily-obscured AGNs, we can expect about 50 Compton-thick AGNs in the SXDS/UDS region above the [OIII] detection limit by assuming similar number of Compton-thick AGNs as Compton-thin type-2 AGNs.

We set the detection limit of the stellar mass limit sample (sample 1, see §5) corresponding to $L_{\rm [OIII]} = 2.8 \times 10^{42}\,{\rm erg\,s}^{-1}$ at $z = 1.5$ with S/N=10, which is equivalent to an unobscured $L_{2-10{\rm keV}} = 1.4 \times 10^{44}\,{\rm ergs}^{-1}$. By detecting H$\alpha$ and [OIII] with S/N$>$ 10, secondary emission lines, such as [NII] and H$\beta$ are expected to have S/N$>$ 3, and hence AGNs can be distinguished clearly from HII regions as shown in Fig. 4 in §2.2. Combining the [OIII]-line selected AGNs with the deep X-ray data in the SXDS/UDS region which reach the detection limit of $L_{2-10{\rm keV}} = 1 \times 10^{43}$ erg s$^{-1}$, we can directly identify heavily-obscured AGNs using the ratio $L_{\rm [OIII]}/L_{2-10{\rm keV}}$ as shown in Fig. 11.

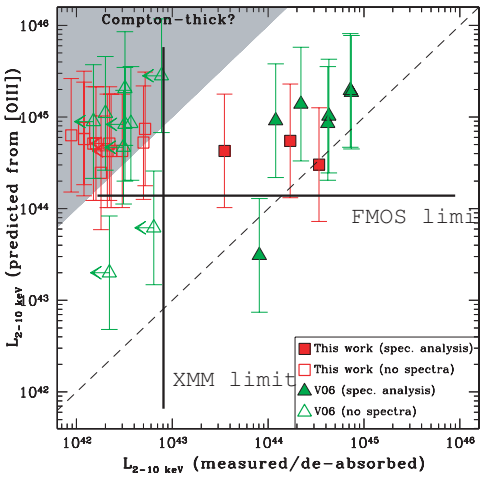


Figure 11 Observed obscuration-corrected hard X-ray luminosity vs [OIII] line luminosity (converted to corresponding X-ray luminosity using L[OIII]-$L_X$ relation) of obscured AGNs found in SDSS (Vignali et al. 2010). The thick vertical and horizontal solid lines indicate the [OIII] and 2–10 keV detection limits in this survey. FMOS can survey statistically candidates of Compton-thick AGNs in the peak epoch similar to those found in the local universe by SDSS.

Searching for strong [OIII] emission may miss obscured AGNs without strong emission lines, such as the fully-covered less-luminous AGNs in the local universe (Ueda et al. 2007, ApJ, 664, 79). However, such objects can be identified among *AKARI* sources with power-law-like mid-IR SEDs which indicate existence of obscured AGN, and/or among submm ASTE/AzTEC sources as well as *Herschel* FIR sources described below. Thus FMOS observations of these sources will provide complementary information on the fraction of heavily-obscured AGNs without strong [OIII] emission line at $z \sim 1$–2. Such weak-lined AGNs may also be identified among radio sources described in section 4.1. There is also a possibility that the mass-limited galaxy sample may miss obscured AGNs in less-massive galaxies, but this population will be detected in observations of less massive galaxies with strong emission lines proposed in this SSP. The complementary structure of the study can only be efficiently proceeded with SSP; individual separate studies would not cover these issues properly.

In summary, our careful selection of samples ensures that we will be able to measure redshifts and hence space densities for all significant populations of AGNs and to relate these to the populations of star-forming and passive galaxies in the same volumes and at the same epochs.

### 3.1.3 Luminosity dependence of obscured AGN fraction

The fraction of obscured AGN depends on AGN X-ray luminosity (e.g., Akiyama et al. 2003, ApJS, 148, 275; Ueda et al. 2003, ApJ, 598, 886); among luminous AGNs the obscured fraction is small, while it is higher in lower luminosity AGNs. This may due to the structure and evolution of the dusty torus. If the AGN activity is high and luminosity is large, the dust may be destructed by the radiation, or the size of the dusty torus would be small, leading to the obscuration fraction smaller. This view may be supported by the fact that dust-to-gas ratios in AGNs often show much smaller values than that seen in interstellar of the Milky Way galaxy (e.g., Watanabe et al. 2004, ApJ, 610, 128).

However, the dependence is not yet fully examined, because it is almost impossible to catch whole population of obscured AGNs. With this SSP, since we will collect such obscured AGNs with various methods, we will be able to examine the more reliable fraction as a function of luminosity. The dependence may change with redshift, phase of evolution of AGNs, and studying these aspects would gives us a clue to unveil formation and evolution of dusty torus as well as AGN/QSO itself.

## 3.2 Unobscured mass assembly of supermassive black holes at $z \sim 2$: accurate estimates of black hole masses and Eddington ratios

Current observational constraints are not strong enough to differentiate between various cosmological models of the mass buildup of SMBHs (e.g., Di Matteo et al. 2008, ApJ, 676, 33) since the bulk of this population has not been adequately assessed in the era of rapid growth. This is because the available data sets, such as the SDSS quasar sample, only probe the high mass end ($M_{\rm BH} > 10^9 M_\odot$) of the black hole mass function (BHMF; Vestergaard & Osmer 2009, ApJ, 699, 800), whose steep decline means it is susceptible to large uncertainties when extrapolated to lower masses. Intriguingly, many models suggest that the bulk of accretion occurs at lower masses ($M_{\rm BH} > 10^9 M_\odot$) and evolves 'anti-hierarchically', possibly in relation to the evolution seen in the galaxy population as a whole (Tamura et al. 2006, MNRAS, 365, 134; Merloni & Heinz 2008, MNRAS, 388, 1011). Therefore, it is imperative to generate statistical samples of AGNs with reliable black hole masses, based on virial estimates, that probe below the characteristic mass (or 'knee') of the BHMF at $z \sim 2$.

X-ray surveys such as the Subaru/XMM Deep Survey (SXDS) and COSMOS are now generating samples of moderate-luminosity AGNs that potentially have masses down to $M_{\rm BH} \sim 10^{7.5} M_\odot$ (e.g., Alexander et al. 2008, AJ, 135, 1968). FMOS

therefore creates the opportunity to measure black hole masses for large samples of spectroscopically-identified broad-line AGNs at $1.3 < z < 2.6$ in these fields using the H$\beta$ emission line. It is worth stressing here that the only this line with reverberation mapping that actually calibrates the scaling relations (Peterson 2010, IAU Symp., 267, 151) and nuclear continuum. Since the difference of the line width of broad-line H$\alpha$ emission is only $\sim 10\%$ of that of H$\beta$ and the difference is systematic (Greene and Ho 2005, ApJ, 630, 122), using the H$\alpha$ emission is also expected to be very useful, which enables us to derive black hole masses even for AGNs with weak H$\beta$ emission (and possibly type-1.8/1.9 AGNs) in the similar or wider redshift range. Our aim is to acquire near-infrared spectra with FMOS of broad-line AGNs to measure robust black hole masses and Eddington ratios, both of which are necessary to answer the fundamental questions regarding SMBHs and their role in galaxy evolution.

We can infer from the BHMF that lower mass black holes ($M_{\rm BH} < 10^9 M_\odot$) at $z \sim 2$ must be undergoing rapid growth in order to match the local distribution (Marconi et al. 2004, MNRAS, 351, 169). While there is an evidence that such low mass black holes in the SDSS at low redshift ($z \sim 0.4$) do reach their respective Eddington ratios (e.g., Steinhardt & Elvis 2010, MNRAS, 402, 2637), there is little knowledge regarding their high redshift counterparts. Furthermore, larger AGN samples with accurate Eddington ratios, especially at low rates, have the potential to strengthen recent claims that the shape (i.e., power-law slope) of the X-ray spectrum is strongly correlated with the Eddington ratio (Shemmer et al. 2008, ApJ, 682, 81; Risaliti et al. 2009, ApJ, 706, L6).

Deriving the Eddington ratios in a wide range of AGN luminosity is also very useful. One interesting application is to apply the Eddington ratio to derive black hole mass in type-2 AGNs, in which nature of host galaxies can be studied owing to its intrinsic obscuration of bright nucleus. This would help the understanding of the co-evolution of galaxies and AGNs as described later. Another interesting possibility is to find a significant number of super-Eddington AGNs in the sample which can be recognized from their H$\beta$, [OIII] and FeII emission as narrow-line Seyfert 1s/QSOs. Since SMBHs grow very rapidly in this epoch, there may be such a bonus finding.

### 3.3 Environment effects on AGN evolution

The environmental dependence described in §2.4 for the galaxy evolution is also expected to be mirrored to AGN/QSO evolution. If the environmental variations are primarily driven by galaxy-galaxy mergers, AGN/QSO activities should also be activated during the processes. This scenario can be tested by comparing the appearance of AGNs/QSOs and the enhanced star forming activities across various environments. The tight correlation between mass of SMBH and stellar mass of spheroid component of its host galaxy indicates the co-evolution of host galaxies and AGNs, and therefore we naturally expect that the fraction of AGN/QSO is the highest when and where star forming activities of galaxies are peaked. Hence the inside-out and down-sizing scenarios may also hold for AGN/QSO evolution.

In fact, the radio-loud QSOs/AGNs are understood to form at high density peaks in the early epoch of the universe. However, the radio-quiet AGNs/QSOs do not necessarily reside in high density regions in the lower redshift universe ($z < 0.1$) (e.g., Miller et al. 2003, ApJ, 597, 142; Sorrentino et al. 2006, A&A, 451, 809). Interestingly, even at $z \sim 1$, there are hints that radio-quiet QSOs reside in the outskirts of clusters and groups (Tanaka et al. 2001, ApJ, 547, 512; Ohta et al. 2003, ApJ, 598, 210). This may be the result of a difference between the feedback mechanisms of radio- and quasar-mode, but the sample sizes of these studies are very small, and the systematic studies of AGNs/QSOs across various environments ranging from general field to cluster core from intermediate redshifts to high redshifts ($z \sim 3$) are crucial to a deeper understanding of the AGN activation and of the co-evolution of AGNs/QSOs and galaxies.

Environmental dependence of the AGN fraction will be examined by locating the non-, mildly-, and heavily-obscured AGN samples in the distribution of the field galaxies. Such studies will be supplemented with the cluster surveys; AGNs found in the clusters can also be used to evaluate the AGN fraction in the highest density environment. Therefore coordinated systematic spectroscopic FMOS survey is crucial to obtain the AGN and non-AGN galaxies in the same volumes and at the same epochs.

## 4 Co-evolution of AGNs/SMBHs and galaxies

In the local universe, the mass of the SMBHs is well proportional to the stellar mass of the spheroid of its host. The tight relation implies the presence of some kind of co-evolution/feedback between SMBHs and galaxies. It is, however, still unknown whether the black-hole growth is earlier than galaxy evolution or vice versa, or almost simultaneous. When and what kind of feedback mechanism occurred is also quite unclear. In theoretical models, there are controversial predictions on the evolution of SMBHs and galaxies. For instance, Croton (2006, MNRAS, 369, 1808) claimed growth of SMBH is earlier without clear mass dependence (upper panels in Fig 12). While Sijacki et al. (2007, MNRAS, 380, 877) predicted earlier growth of stellar mass and the presence of mass dependent evolution (lower panels in Fig 12). With FMOS, in this unified SSP studying AGN and galaxies we will examine when and how co-evolution/feedback mechanism worked in the epoch where the SMBHs as well as galaxies evolve very violently.

### 4.1 Massive galaxy formation and the onset of radio-mode feedback

It is now generally accepted that AGNs play a major role in shaping the evolution of their host galaxies, via a process known as 'AGN feedback'. This feedback can take one of two forms, for which Croton et al. (2006, MNRAS, 365, 11) coined the terms 'quasar mode' and 'radio mode'. Quasar mode feedback occurs when the central SMBH is accreting close to its Eddington

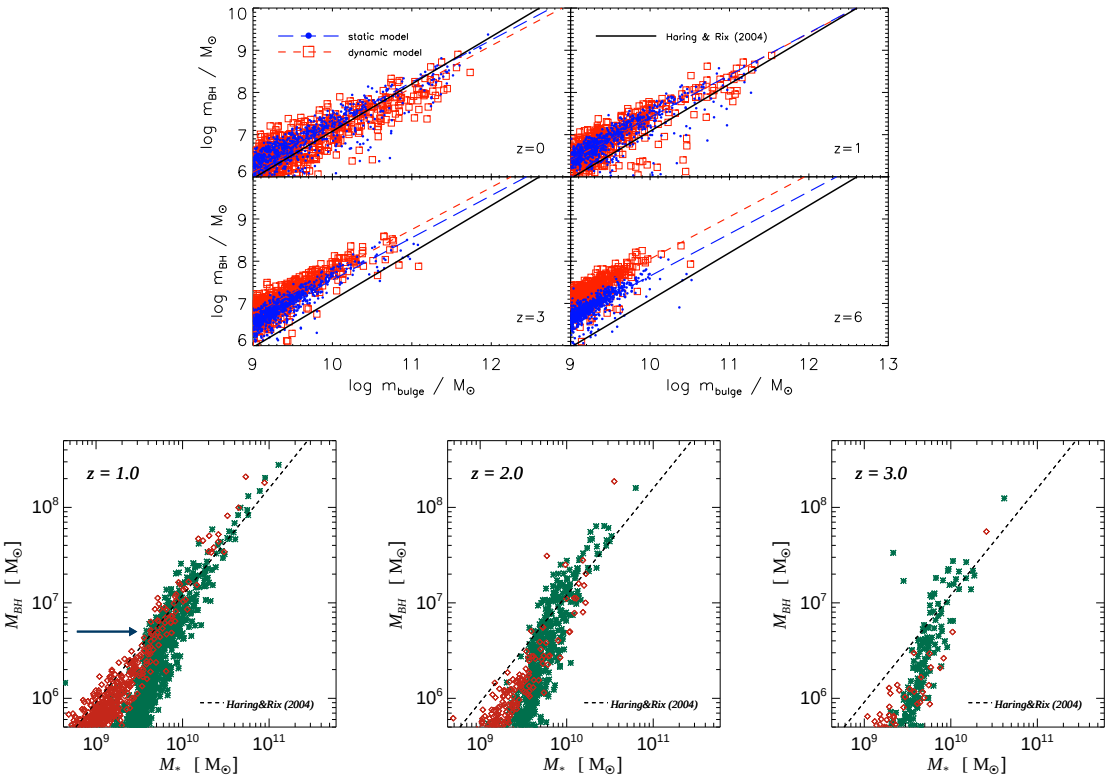


Figure 12 Predicted SMBH-bulge mass relation in simulations. Upper panels by Croton (2007) and lower panels by Sijacky et al. (2007). Determining masses of SMBHs in AGNs at $z \sim 1-2$ is expected to discriminate which model (or other model) is valid to explain the blackhole mass and stellar mass relation at the redshift, hence what kind of feedback was actually working.

limit, and the infalling material forms a hot accretion disk that, in turn, ionizes the surrounding gas to produce a rich emission-line spectrum. This mode is associated with mergers and interactions which also promote star formation, although the precise relationship between the accretion and star-formation activities is not fully understood.

In contrast, the physics and energetics of radio mode feedback are far clearer. This mode occurs when hot gas accretes directly onto the black hole at a low rate, eliminating the need for an accretion disk, and hence not producing strong emission lines (note that classical powerful radio galaxies such as Cygnus A are actually 'quasar mode' systems). Best et al. (2005, MNRAS, 362, 25) demonstrated that the fraction of galaxies hosting a low-luminosity radio-loud AGN was a strong function of stellar mass. Inferring this to be a duty cycle of activity, Best et al. (2006, MNRAS, 368, L67) showed that the energy output (making plausible assumptions about the relationship between radio luminosity and kinetic power) precisely balanced the observed X-ray cooling. This mechanism, whereby radio 'bubbles' inflate cavities in the surrounding hot X-ray halo (as clearly seen in, e.g., the Perseus cluster; Fabian et al. 2003, MNRAS 344, L43; Fabian et al. 2006, MNRAS, 366, 417) is therefore responsible for the curtailment of baryonic cooling and hence star formation in massive galaxies, and explains the steep cut-off at the bright end of the galaxy luminosity function.

Radio mode feedback only becomes important once massive elliptical galaxies have formed, and therefore it can be used to locate the epoch of massive galaxy assembly. This is still a major problem in modern cosmology, as the existence of massive galaxies at high redshift continues to present difficulties for models of galaxy formation (e.g., Collins et al. 2009, Nature, 458, 603; Stott et al. 2010, ApJ, 718, 23). Blank-field surveys for massive galaxies are hampered by the reliance on photometric redshifts and stellar mass estimates, and hence their results are open to debate without extensive confirmational spectroscopic follow-up (see, e.g., van Dokkum et al. 2006, ApJ, 638, L59). By comparison, identifying the epoch beyond which there is a decline in the number of low-luminosity radio sources will pinpoint the time at which the most massive galaxies have just completed their stellar build-up and found equilibrium between gas cooling and radio-source heating. Locating this epoch provides an essential constraint for models of galaxy formation. Detecting such a decline requires far less follow-up and, indeed, has been tentatively seen in the SXDF/UDS sample of 505 radio sources (Simpson et al. 2011, in prep.; Fig. 13). However, this result also hinges on the reliability of photometric redshifts, and is also made slightly ambiguous by the overlap between low-luminosity radio-loud AGN and high-luminosity radio-quiet (quasar mode) sources, although these evolve like the luminous AGN population and so are expected to peak at $z \sim 2.5$.

FMOS is the ideal instrument to tackle this problem, since it is able to detect the strong 4000-Å break in massive galaxies at $z \sim 2$ with little or no line emission, and also detect the strong emission lines of [OII] and/or [OII] at this redshift to eliminate contaminating quasar-mode radio-quiet objects. Since the population we are interested in does not have strong accretion, there is no hot dust emission longward of 1 $\mu$m and the *Spitzer*/IRAC colours provide robust (if rather uncertain) photometric redshift

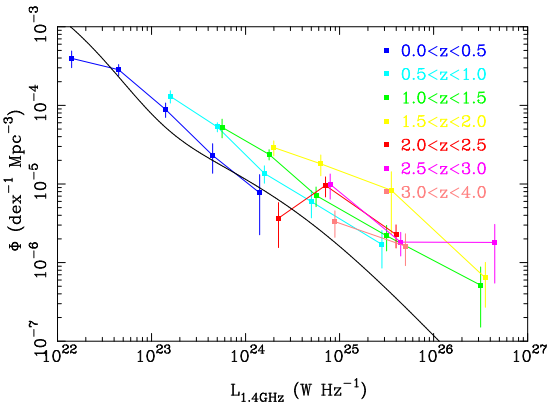


Figure 13 Evolution of the radio luminosity function with redshift. Different colour symbols denote different redshift ranges as indicated in the key, while the black solid line is the parameterized fit to the local radio luminosity function of Mauch & Sadler (2007). Bins are of of width $\Delta \log L_{1.4\mathrm{GHz}} = 0.5$ for $L_{1.4\mathrm{GHz}} \leq 10^{25}\,\mathrm{W\,Hz^{-1}}$ and $\Delta \log L_{1.4\mathrm{GHz}} = 1.0$ at higher luminosities. Points representing different redshift bins are offset horizontally for clarity. The tentative decline seen in the radio luminosity function at $2.0 < z < 2.5$ (red points) is consistent with a picture where massive ellipticals have just formed at this epoch and begin 'radio mode' feedback. However, this result needs confirmation from a larger spectroscopically-confirmed sample, which only FMOS can provide.

estimates (Simpson & Eisenhardt 1999, PASP, 111, 691). By selecting radio sources with appropriate colours from the deep IRAC observations in the SXDS/UDS and/or COSMOS fields and measuring spectroscopic redshifts using the 4000-Å break, we will reliably and efficiently measure the evolution of the radio-mode galaxy population and hence determine when the most massive galaxies have fully assembled.

## 4.2 Mass-accretion rate vs star-formation rate

Another important aspect for the understanding of the co-evolution is to derive and compare mass-accretion rate onto a SMBH and star-formation rate in an AGN host galaxy. If the co-evolution proceeds exactly the same timing, the ratio of mass-accretion rate to star-formation rate should be the same as the mass ratio of SMBH and spheroid component. Of course, there is probably a possibility that black hole growth delays after the star burst or star-formation activity is suppressed after AGN ignition. Thus the ratio between accretion rate and star-formation rate in an AGN host may be different from the mass ratio of SMBH and its host. Comparing the mass-accretion rates with star-formation rates in AGN hosts and with those in non-AGN galaxies with the same stellar mass, we can tackle the problem.

It is generally hard to estimate star-formation rates in AGN hosts. However we can do it by using [OII]3727 luminosity. Although the [OII]3737 luminosity is a mix from star formation and AGN, the contribution from AGN can be estimated from [OIII]5007 emission (Silverman et al. 2009, ApJ, 696, 396). The ratio of [OII]/[OIII] for AGNs decreases with increasing [OIII] luminosity, i.e., a contribution from star formation exists provided that [OIII] is a good indicator of AGN luminosity. Thus we can subtract the AGN contribution from the observed [OII] luminosity. (When the target AGNs are located at high redshifts and [OIII] emission line is out of the observed wavelengths, the [OIII] luminosity due to AGN can be estimated statistically from X-ray luminosity.) Silverman et al. (2009) claimed at $z \sim 1$ that the star-formation rates in their AGNs are higher than those of star-forming galaxies in the same stellar mass range on average, supporting e.g., simulation results by Di Matteo et al. (2005, Nature, 433, 604). They also found the mass accretion onto SMBHs has a week correlation with star-formation rates, and the median value of the ratio is $2 \times 10^{-2}$, about one order of magnitude larger than that of a SMBH against stellar mass of a spheroid component. This is consistent with the view SMBHs grow during the AGN phase. The value is also comparable to that in a phase after reaching peak accretion rate (Di Matteo et al. 2005). With FMOS we can extend this study up to $z \sim 2 - 2.5$, about $2 - 3$ Gyr earlier than $z \sim 1$, with a larger sample.

Recently, Hatziminaoglou et al. (2010, A&A, 518, L33) separated star-formation activity and AGN activity by combining *Spitzer*/MIPS and *Herschel*/SPIRE data and derived star-formation rates and mass-accretion rates in AGNs. Once we obtain redshifts for the dusty objects found with $AKARI$, ASTE/AzTEC, and *Herschel*, we may be able to know both the star-formation rates and mass-accretion rates in the galaxies.

Furthermore, we compare colors of host galaxies, which enables us to examine track of evolution. Recently, Hasinger (2008, A&A, 490, 905) proposed an evolutional track of galaxy and AGN: A galaxy evolve from the blue cloud to the red sequence, and rejuvenation due to the accretion of fresh gas from the surrounding of a galaxy may be a cause for the AGN activity moving its position to the so-called green valley. Meanwhile there is a scenario that AGN activation occurs among (rather massive part of ) the blue cloud going into the green valley and eventually it moves to the red sequence. In order to discriminate the scenario, it is necessary to investigate star-formation activity and properties of its host (not only stellar mass, but also D4000 break from SED, age, extinction from SED analysis in AGN phase and in non-AGN phases together). Although it would not be straightforward to extract properties of AGN host, we can examine them for obscured AGNs thanks to its intrinsic obscuration of a bright nuclear

light and for weak AGNs. Comparing these properties with those for non-AGN star-forming galaxies, we may be able to have insights for the passes to AGNs and to non-AGN galaxies and origin of AGN activity as well as the feedback mechanism.

### 4.3 Metallicity in narrow-line regions

Metallicity in narrow-line regions (NLRs) may be another key for examining the co-evolution scenarios. Metallicity studies can be made not only for star-forming galaxies as described in §2.2, but also possible for NLRs in AGNs. Since the NLRs are located in the innermost regions of galaxies, if the metallicity of NLRs in AGNs is significantly higher than that of non-AGN star-forming galaxies as a whole at the same stellar mass, the galaxy evolution occurred more preferentially in the inner part of a galaxy, i.e., inside-out manner. Revealing this manner of evolution at the target redshifts may give us a new clue to understand the process of the co-evolution.

The SDSS data suggest that most AGNs in the local universe have super-solar metallicity, and AGNs with solar metallicity or below are extremely rare (only $\sim$0.2%; Groves et al. 2006, MNRAS, 371, 1559). At higher redshifts, any cosmological evolution of the NLR metallicity has not been reported, based on samples of a few dozens of type-2 AGNs (Nagao et al. 2006, A&A, 447, 863; Matsuoka et al. 2009, A&A, 503, 721). Since the absence of any redshift evolution in the NLR metallicity appears contradictory to the behaviors of metallicity in star-forming galaxies, systematic measurements of NLR metallicity for much larger numbers of AGNs are required. Groves et al. (2006) used diagnostic flux ratios of H$\alpha$, H$\beta$, [NII], and [OIII] to investigate the NLR metallicity, which can be applied also with FMOS observations by focusing on AGNs at $1.3 < z < 1.6$.

## 5 Samples and observing plans

To achieve the above scientific aims, it is clearly necessary to construct a sample covering wide ranges of parameters related to galaxy and AGN population. Although traditional spectroscopic surveys adopt magnitude limit selections, such a way is not efficient to unveil the evolution of galaxies and AGNs in the epoch due to a large contamination by foreground galaxies and to the detection limit of the instrument. Therefore, in this SSP, we target

1) Core-sample of 5,000 galaxies which are selected by stellar mass and apparent star formation rate, and

2) 6 Extend-samples covering parameter spaces with lower or no starformation activity (Extend-sample 1 and 2), lower stellar mass (Extend-sample 3), larger dust obscuration (Extend-sample 4), AGN activities (Extend-sample 5), and environment with higher local density (Extend-sample 6).

Only with the core sample, the results can be heavily biased: using the apparent star-formation rate limited sample can introduce a bias against dusty galaxies which tend not to be detected even if the intrinsic star-formation rate is the same. Adding the extend-samples, we can evaluate such biases covering wide parameter ranges effectively. This kind of coordinated studies would be hard to achieve, if each sample is instead to be observed independently by separate group. This is an advantage of organizing FMOS SSP. The details of the core and extend-samples are described in the next subsections.

The samples are constructed mainly in fields which are very well studied in multiwavelengths including extensive optical spectroscopic surveys, i.e. Subaru XMM-Newton Deep Survey (SXDS) and COSMOS fields. The SXDS is almost identical to the UKIDSS Ultra Deep Survey (UDS) field, and this field has been developing under collaboration between UK and Japan. In order to extend the samples to galaxies with dusty star formation, we also choose *AKARI* Deep Field (ADF) where $AKARI$ deep survey has been conducting. The field is also developed by UK and Japan, and observations with *Herschel* may be done. It should be noted that the three fields cover whole right ascension (at EL $> 30^{\circ}$) without overlapping. Additionally, to extend the samples to galaxies in very high density regions, we employ well studied clusters of galaxies distributed over the wide range of right ascension. Furthermore, to reduce the cosmic variance and to use observing time as effectively as possible, we set samples in supplementary fields: *Chandra* Deep Field-South (CDF-S), Subaru Deep Field (SDF), and All-wavelength Extended Groth strip International Survey (AEGIS).

In the descriptions below, technical feasibility is based on the values in the FMOS web site at Subaru observatory, which are obtained with past engineering observations, i.e., S/N$= 5$ for an emission line (narrow emission) flux in the $1.2''$ diameter fiber aperture of $1 \times 10^{-16}$ erg s$^{-1}$ cm$^{-2}$ with an exposure time of 1 hour in the low-resolution mode ($R \sim 500$, LR). For the high-resolution mode ($R \sim 2200$, HR), the throughput is $1.5 - 4$ times higher than that in the LR mode according to the FMOS web site, but the actual capability is being examined in engineering runs. Usually we will use the cross-beam switch mode; in the first exposure, 200 objects are allocated to fibre spines and the other 200 fibres take sky spectra, and then in the second exposure the former 200 fibres take sky and the latter 200 fibres are allocated to the same target objects. This reduces the number of targets which can be observed simultaneously, but can achieve more accurate sky subtraction, leading to effectively good performance. In the calculation of expected observing time, we assume $40 - 50\%$ overhead and $75 - 80\%$ fraction for the clear sky condition based on the Subaru web site.

### 5.1 Core-sample: stellar-mass and flux limited sample

The core sample is selected based on stellar mass and expected fluxes of Balmer emission lines. The expected flux limit is introduced in order to detect diagnostic emission lines within reasonable integration time. The core sample consists of two

subsamples, one selected based on photometric redshift estimation (Phot-z sample) and the other selected using spectroscopic redshift information (Spec-z sample). The latter sample is more secure for line detection, but the redshift range and the number is limited and probably biased toward objects with less dust extinction. Therefore the Phot-z sample is inevitable as the base-line sample to understand the galaxies in the peak epoch, and the sample is supplemented with the Spec-z sample.

### 5.1.1 Phot-z sample

The sample is selected from galaxy catalogs with $K_{\rm AB} < 23.9$ mag with a stellar mass larger than $10^{9.5} M_\odot$, an expected emission line flux larger than (a few $-20$) $\times 10^{-17}$ erg s$^{-1}$ cm$^{-2}$, and $0.7 < z_{\rm ph} < 2.5$. For the redshift range of $1.4 < z_{\rm ph} < 2.5$, the BzK method may be used as a supplementary discriminator.

The sample is constructed in SXDS/UDS and COSMOS fields, and supplementary in SDF. Using multi-wavelength datasets in these fields, photometric redshift is estimated for each K-band selected galaxy. The intrinsic star-formation rate and dust extinction, E(B-V), are calculated with apparent $L_{\rm UV}$ and UV continuum slope. The expected emission-line flux is calculated using the intrinsic star-formation rate and E(B-V). The E(B-V) for stellar component is converted to that for ionized gas component using the prescription by Cid Fernandes et al. (2005, MNRAS, 358, 363) (essentially same as that by Calzetti et al. 2000, ApJ, 533, 682). Alternatively, the expected line flux may be calculated from the star-formation rate, dust extinction, and $z_{\rm ph}$ of the best fit population synthesis model spectrum to the observed spectral energy distribution.

The sample is used for studies of star-formation rate, amount of extinction (when H$\beta$ is detected), specific star-formation rate, and gas metallicity together with their dependence on stellar mass, etc. There are three subsamples in the sample depending on target redshift ranges and target emission lines:
**A. (N2 sample):** $f({\rm H}\alpha) > 2.0 \times 10^{-16}$ erg s$^{-1}$ cm$^{-2}$ (SN=10), $z_{\rm ph} = 0.7 - 1.3$, covering [NII]-H$\alpha$: $\sim 1100$ objects/FoV.
**B. (O3N2 sample):** $f({\rm H}\alpha) > 5.0 \times 10^{-17}$ erg s$^{-1}$ cm$^{-2}$ (SN=5), $z_{\rm ph} = 1.3 - 1.6$, covering [NII]-H$\alpha$ and [OIII]-H$\beta$: $\sim 1800$ objects/FoV.
**C. (R23 sample):** $f({\rm H}\beta) > 3.0 \times 10^{-17}$ erg s$^{-1}$ cm$^{-2}$ (SN=5), $z_{\rm ph} = 1.7 - 2.4$, covering [OIII]-H$\beta$ and [OII]: $\sim 80$ objects/FoV
It is necessary not only to detect the strongest line such as H$\alpha$, but also to detect (or to put sufficient upper limit on) secondary emission lines such as [NII] to conduct line-ratio diagnostics. The above selection limits for the Balmer lines are determined to detect forbidden lines, i.e. [NII], [OIII], [OII], as well with sufficient SN for line ratio diagnostics. It should be note that the [OII] and [OIII] fluxes for sample C are larger than the H$\beta$ flux in the expected metallicity (stellar mass) range.

The detection limits for Balmer lines corresponds to apparent star-formation rates as follows. For the sample A (N2), an H$\alpha$ flux of $2 \times 10^{-16}$ erg s$^{-1}$ cm$^{-2}$ corresponds to $\sim 5 M_\odot$ yr$^{-1}$ at $z \sim 1.0$. For the sample B (O3N2), an H$\alpha$ flux limit corresponds to $\sim 5 M_\odot$ yr$^{-1}$ at $z \sim 1.5$. For the sample C (R23), since the aimed emission line is expected to be weak, we set the relatively lower flux level; if there is no obscuration, the corresponding star-formation rate is $\sim 17 M_\odot$ yr$^{-1}$ at $z = 2.0$.

Metallicity for each object will be examined three line ratio diagnostics depending on target redshift. With use of samples A and B, we can derive gas metallicity evolution during the period between $z \sim 0.7$ to 1.6; i.e., the cosmic age of 3.9 Gyr to 7.2 Gyr is covered with the same method (H$\alpha$/[NII]). This is ideal for tracing evolution of metallicity, because the relative calibration problem in metallicity indicator (Kewley and Ellison 2008, ApJ, 681, 1183) prevents us from charting chemical evolution with the same method, and no other such studies have been made. We have to be careful with the presence of metallicity gradient for fixed aperture spectroscopy with FMOS when tracing metallicity in a wide range of the redshift. The sample C can be used for metallicity at $z \sim 2$ ($\sim 1$ Gyr earlier than that at $z = 1.6$). The R23 method gives two metallicities at a fixed value of R23 (= $(I_{\rm [OII]} + I_{\rm [OIII]})/I_{\rm H\beta}$). However, the target stellar mass is larger than $10^{9.5} M_\odot$ and thus the higher metallicity branch (12 + log(O/H) $> 8.0$) is expected to be applicable. This point can also be examined using simulations such as those in Jabran Zahid et al. (2010, arXiv 1006.4877). Unfortunately, with the current configuration of FMOS, we cannot cover the wavelength region from [OII]3727 to H$\alpha$ simultaneously.

To derive star-formation rate and metallicity, we need to distinguish star-forming galaxies and AGNs, and evaluate the strength of Balmer absorption lines of stellar continuum. The discrimination will be made using traditional emission line diagnostic [OIII]5007/H$\beta$ vs [NII]6584/H$\alpha$ (Fig 4 left) for $z = 1 - 1.6$. For the lower redshift ($z = 0.7 - 1.5$), [NII]6584/H$\alpha$ vs [SII]6717+6731/H$\alpha$ is used (Fig 4 middle). For the higher redshift ($z = 1.7 - 2.4$), [OIII]5007/H$\beta$ vs [OII]3727/H$\beta$ diagram (Sobral et al. 2009, MN, 398, 75; Fig 4 right). The presence of [NeV]3426 emission can also be used to isolate AGNs. Stellar photospheric Balmer line absorption, which affects the derived flux of Balmer emission lines, will be estimated based on the SED fitting; best fitted SED fitting can produce spectrum of each target galaxy.

Since the numbers of galaxies meeting the above criterion are huge, we will randomly select from the original samples. In SXDS, for the sample A (N2 sample), since we like to explore redshift evolution at least in two epochs, to obtain 5 data bins along the stellar mass, and to explore a dependence on another parameter such as star-formation rate at least with 3 data bins, we will have 30 bins for the sample. At each bin we like to achieve S/N of 5, thus 25 objects in each bin. This gives $\sim 750$ targets, but by considering a success rate, we would like to observe $\sim 2000$ objects. As for the sample B (O3N2 sample), we only need one redshift bin, and thus totally 15 bins are necessary. Similarly we would like to observe $\sim 900$ objects. The sample C is not large and we can observe all the targets.

In the SXDS field, we put higher priority to the region where *HST*/WFC3 observations are scheduled. In the COSMOS field, with this sample we focus on its central square degree where both *HST*/ACS image for morphological inspection where $\sim 5,000$ spectroscopic redshifts at $1 \lesssim z \lesssim 3$ and $\sim 20,000$ spectroscopic redshifts at $z < 1$ are already available from the zCOSMOS-Deep and zCOSMOS-Wide data, respectively. It is worth noting that the high completeness already achieved by zCOSMOS at $z < 1$, while that the quite low success rate of zCOSMOS-Deep ($\sim 25\%$) at $1 \lesssim z \lesssim 1.6$.

The number of required nights for SXDS is:
A. $\sim$ 2000 / 200 $\times$ 2.5 hrs $\times$ 1.5 / 0.75 = 50 hrs = 6.3 nights
B. $\sim$ 900 / 200 $\times$ 4.0 hrs $\times$ 1.5 / 0.75 = 36 hrs = 4.5 nights
C. $\sim$ 260 / 200 $\times$ 11.1hrs $\times$ 1.5 / 0.75 = 28.9 hrs = 3.6 nights
Totaling $\sim$ 14.4 nights in SXDS. For the COSMOS similar numbers will be needed.

Since there are still various uncertainties for feasibility for these targets, we like to start observations with more promising candidates. Based on the results of a first few runs, the subsequent strategy can be modified.

#### 5.1.2 Secure sample with optical $z_{\rm spec}$

Samples with only photometric redshifts (such as those described above) may be ambitious for the early days of our proposed FMOS survey. We thus employ a sample with accurate redshifts from optical spectroscopy based on stellar mass (but in $I-$band selection). Although our target redshift range is 'redshift desert', the redshift up to $z \sim 1.4$ can be covered with optical spectroscopy where [OII] emission is detected in $\lambda \sim 9000$ Å (Fig 2). By selecting those galaxies with reliable redshifts where H$\alpha$ is in a clean part of the spectra (i.e., without OH airglows) and in high sensitivity regions, we can obtain accurate flux measurements. The sample is to use deriving star-formation rate from H$\alpha$ luminosity (corrected for dust extinction if H$\beta$ can be measurable), and can also be used for derivation of gas metallicity. Of course, the emission line observed in the optical wavelength may be quenched due to dust obscuration and may bias to unobscured objects, but this can provide us a sample with which to examine the star-formation activities and gas metallicity at the epoch. There are several candidate fields, among them here we choose the COSMOS field and supplementary AEGIS and CDF-S considering the presence of deep *HST* images (and *Spitzer* images in CDF-S).

With accurate spectroscopic redshifts, it would be better to employ the high resolution mode (HR; $R \sim 2200$) to identify emission lines effectively, because the system throughput of the HR mode is 1.5–4 times higher than low resolution mode(LR; $R \sim 500$) at all wavelengths. With the HR mode, the velocity resolution is $\sim$ 150 km s$^{-1}$ and we can constrain dynamical masses especially in fields where *HST* imaging is available. In this regard, the COSMOS field as well as AEGIS and CDF-S are suitable fields.

There are $\sim$ 600 such targets at $z > 0.7$ in the COSMOS field. Our goal is to explore star-formation rates as low as $2-4\,M_\odot\,{\rm yr}^{-1}$ at $z \sim 1-1.5$, corresponding to a flux of $\approx 5\times10^{-17}$ erg s$^{-1}$ cm$^{-2}$. A line with FWHM$\sim 100\,{\rm km\,s}^{-1}$ of this luminosity can be detected at the $5\,\sigma$ level in $\sim 4$ hours (including overheads and a clear night fraction), using the HR mode. We aim to use the HR mode for targets with accurately determined redshifts because the system throughput of HR mode is 1.5–2.0 times higher in $J$ band and 2–4 times higher in $H$ band than those of LR mode. Here we assume that the sensitivity of HR mode is two times higher than that of LR mode. With cross-beam switch mode, for each FMOS observation we will target 200 galaxies with 4 hour. This number would be provide excellent pilot studies in the epoch. Total number of nights is 3 FoVs $\times$ 4 hour observing time, that is, 1.5 nights.

### 5.2 Extend-sample 1: stellar-mass limit galaxies

In order to examine the star formation and AGN activities more completely among massive galaxies, we supplement the core-sample with the extend-sample 1 galaxies selected only with stellar mass. The core-sample uses apparent line flux derived from the UV properties, but such selection can miss some populations of star-forming galaxies due to uncertainties of star-formation rate estimates, and properties of dust extinction, and can introduce biases. Such biases can be evaluated by having a pure stellar-mass limit sample. Moreover, obscured AGN activities (particularly the Compton-thick AGNs which can also be missed in the X-ray surveys) can reside in galaxies with weak/no star-formation activity; such objects should have strong emission line due to the AGN activity, but can be missed in the core-sample selection.

This sample targets galaxies with stellar mass larger than $10^{10.5}M_\odot$ at $z_{\rm ph} = 1.3-1.6$ selected from the SXDS catalog mentioned above. The number of the galaxies in this sample is $\sim$ 3600. The stellar mass limit of $10^{10.5}M_\odot$ is set by following the result by Yamada et al (2009, ApJ, 699, 1354) that among $M_* > 10^{10.5}M_\odot$ the fraction of AGNs is large. It is also intriguing to note that the cosmic star-formation rate density peaks at around the mass based on '[OII] luminosity' at $z \sim 1$ (Gilbank et al. 2010, MNRAS, 405, 2594). Unfortunately, if we take a wide range of stellar mass and redshift, the sample size is extra-ordinary and the observing time is unrealistically huge. Thus in this study we choose the mass range larger than $10^{10.5}M_\odot$. The redshift range of $1.3-1.6$ is suitable because we can cover both H$\alpha$ (and [NII]) and H$\beta$ (and [OIII]).

We set a detection limit of $1.3\times10^{-16}$ erg s$^{-1}$ cm$^{-2}$ (flux within the 1.2″ fiber aperture with SN=10 for an effective integration time of 2.5 hour). This detection limit corresponds to an apparent star-formation rate of 13 $M_\odot$ yr$^{-1}$ for H$\alpha$ in star-forming galaxies or an unobscured X-ray luminosity of $1.4\times10^{44}$ erg s$^{-1}$ for [OIII] in AGN at $z = 1.5$. By detecting H$\alpha$ and [OIII] with S/N$>$ 10, secondary emission lines, such as [NII] and H$\beta$ are expected to have S/N$>$ 3, and hence AGNs can be distinguished clearly from HII regions as shown in Fig. 4 in §2.2. Combining the [OIII]-line selected AGNs with the deep X-ray data in the SXDS/UDS region which reach the detection limit of $L_{2-10{\rm keV}} = 1\times10^{43}\,{\rm erg\,s}^{-1}$, we can directly identify heavily-obscured AGNs using the ratio $L_{\rm [OIII]}/L_{2-10{\rm keV}}$ as shown in Fig. 11.

In this sample, we expect that individual star-formation rate can be derived for about 400 (S/N = 10 for H$\alpha$) or more galaxies. These numbers would be good enough if we construct H$\alpha$ luminosity function with 5 stellar mass or luminosity bins with 100 (S/N$\sim$ 10) galaxies at the redshift in question (i.e., 500 galaxies). About half of the sample have MIPS counterparts, which make it possible to combine non-obscured star-formation rate and obscured star-formation rate. Then star-formation rate and

specific star-formation rate against stellar mass can also be examined. We can further expand the sample size to include less massive star-forming galaxies at lower and higher redshifts as described below. Thus the trend we will see with this sample can be examined with respect to a wider range of stellar mass parameter space and redshift parameter space.

Among $\sim 3600$ objects in the SXDS, we randomly select half of them. Thus required observing nights is 1800/200 FoVs $\times$ 3.6 hours (incl.overhead) / 0.75 (weather) = 43.2 hours = 5.4 nights.

## 5.3 Extend-sample 2: Passive galaxies

The core-sample and extend-sample 1 aim at detecting the emission lines and their integration time is not long enough to detect stellar continuum emission with sufficient S/N. The extend-sample 2 is designed to extend the sample to no star-formation activity by absorption lines. Using the sample, formation epoch or a period from the last star formation will be evaluated for massive passive galaxies.

The sample is selected with pBzK selection supplemented with photometric redshifts. With the current sensitivity of FMOS, we have to concentrate on the brightest galaxies in the field to detect its continuum. Considering the continuum detection limit, $J$-band magnitude limit of $J_{\rm AB} < 22$ mag will be applied. In order to escape from contamination by dusty star-forming galaxies and obscured AGNs, objects with dust thermal emission are excluded.

Effective integration of 10 hours is necessary for a passive galaxy with $J_{\rm AB} < 22$ mag to detect their continuum with ${\rm S/N} \simeq 10$ after 4 pix binning in wavelength direction. Since the surface number density of pBzKs is estimated as $\simeq 0.07$ arcmin$^{-2}$, we can put $\lesssim 50$ pBzKs as fibre fillers of star-forming galaxies and AGNs proposed in other sections, and keep integrating to an order of $\simeq 10$ hours by putting a fibre to the same pBzK if the fibre configuration in the same field for star-forming galaxies changes after some integration of $< 10$ hours. Therefore, utilizing the wide field and high multiplicity of FMOS through the SSP program, we can effectively observe rare but demanding high-$z$ passive galaxies very efficiently.

## 5.4 Extend-sample 3: Low-mass galaxies

In order to investigate star-formation activities and metallicity at even lower stellar masses, we extend the sample to galaxies selected with line emission, i.e. line emitters, which are good tracers of very low stellar-mass systems, potentially the building blocks of massive galaxies at later times. These emitters are also good probes to studies less dusty environments in galaxies. The samples are selected by emission line surveys with narrow-band filters. The sample consists of four subsamples selected with various narrow-band filters covering a wide redshift range in total. They are summarized as below.

**A. Subaru/Suprime-Cam [OII] emitters at $z = 1.47$ and $1.62$ in SXDS (and SDF)**, which will allow us to study star formation and metal enrichment of low-mass galaxies with a full set of the major nebular lines up to H$\alpha$ and [NII]. Moreover, similar [OII] emitters at $z = 1.5-1.6$ but in cluster fields are also observed in this FMOS SSP (§2.4). The observations for [OII] emitters in general fields will provide a control sample, indispensable for studies of environmental effects in galaxy evolution.

**B. Ly$\alpha$ emitters (LAEs) at $z = 2.18$ in SXDS and COSMOS (and CDF-S).** The observations of them will allow us to constrain metallicity of LAEs, and to examine the metal poor starburst scenario of LAEs. By using the $R_{23}$ method and [NeIII] method, the constraint on metallicity will address the long-standing question about the physical origin of strong Ly$\alpha$ emission from LAEs ($EW_0 = 200-500$Å) that could be produced by very massive early-type stars in metal-poor and/or young starbursts, and/or a geometry of ISM such as that known as Neufeld's clumpy cloud model.

**C. KPNO-CTIO/NEWFIRM H$\alpha$, [OIII], H$\beta$, and [OII] emitters at $z = 0.81-2.18$ in SXDS and COSMOS (and CDF-S).** Because the NEWFIRM emission line galaxies at $z = 0.81 - 2.18$ are identified with a narrow-band (NB) filter in $J$-band, these galaxies are complementary unbiased emitters with the same wavelength for the detection and spectroscopy. Because the wavelength coverage of the NEWFIRM NB ($\lambda = 1.181 - 1.192\mu$m) lies next to that of HiZELS NB ($\lambda = 1.204 - 1.219\mu$m; Sobral et al., 2009, MNRAS, 398, 75) with no overlap, observations of NEWFIRM emitters will trace large-scale structures along the line of sight, as like the case for the LAEs at $z \sim 5$ shown by Shimasaku et al. (2004, ApJ, 605, L93).

**D. UKIRT/WFCAM H$\alpha$ emitters (HAEs) at $z = 0.84$, 1.47, and 2.23 (at $\lambda 1.21\mu$m, $\lambda 1.62\mu$m, and $\lambda 2.12\mu$m, respectively) (HiZELS) in SXDS and COSMOS.** These provide good tracers for studying star-formation rate density at the violent evolution epoch. Spectroscopy with FMOS will make clean samples without interlopers which enables us to derive more reliable H$\alpha$ luminosity function and thus star-formation rate density at the epoch. Further, we can constrain properties of emitters such as described above with similar techniques. Since the [OII] emitters at $z = 1.47$ above also would be H$\alpha$ emitters at the redshift, it is very intriguing to compare these two samples in SXDS to examine the difference and similarity between the two samples.

The Narrow-band filters and targets are summarized in Table 3 and Table 5.

It is worth stressing that these emitters are obtained by narrow-band imaging surveys with Subaru/Suprime-Cam (FoV:34'$\times$27'), KPNO-CTIO/NEWFIRM (FoV:27.6'$\times$27.6'), and UKIRT/WFCAM (FoV $\sim 30' \times 20'$ in one tile), the FoV is well-matched to FMOS. The HiZELS imaging in the SXDS and COSMOS fields already covers regions of 1 sq. degree in each field. It is noted that the samples of [OII] emitters at $z = 1.62$ (sample A) in the SXDS and NEWFIRM emitters (sample C) in the COSMOS field are limited to one pointing region of $\sim$0.2 deg$^2$ and that narrow-band imaging with NEWFIRM in the CDFS will be performed in the near future.

For samples A, B, and C, we define two classes of targets, target-1 and target-2. Target-1 consists of bright emitters whose H$\beta$ line, the weakest among the major nebular lines, is detectable on an individual basis. Target-2 is used for faint emitters from

which we expect to detect any of the major nebular lines. For sample D, since the emission lines are detected in NIR and the flux level matches FMOS sensitivity well, we don't separate the sample into two classes. Since the redshift range is very narrow for emitters, the HR mode is used. Fig 14 shows the target wavelength ranges for samples A, B, and C with the major nebular lines can be covered only by two bands of HR mode. The HR mode keeps the highest throughput in the most important region of the $H$-band, between 1.55$\mu$m and 1.75$\mu$m. Again a better spectral resolution can constrain dynamical masses and distinguish between nebular lines originating from star-forming regions ($\lesssim 300-400$ km s$^{-1}$) and galaxy outflows ($\sim 1000$ km s$^{-1}$).

We estimate the expected fluxes of emission lines as follows. For [OII] emitters, we use the observed line ratios for star-forming galaxies at $z \sim 1.4$ (Maier et al., 2006, ApJ, 639, 858) to infer H$\beta$ and H$\alpha$ line fluxes from [OII] fluxes obtained by narrow-band imaging. [OII] emitters of target-1 are selected from both samples of [OII] emitters at $z = 1.47$ and 1.62 due to the low number density of bright emitters. Target-1 sample has 54 [OII] emitters with the expected H$\beta$ flux larger than $4.2 \times 10^{-17}$ erg s$^{-1}$cm$^{-2}$ per FMOS pointing. [OII] emitters of target-2 are selected from only a sample of [OII] emitters at $z = 1.47$ as objects with the detectable H$\alpha$ flux. Among the faint emitters, we target 150 [OII] emitters per FMOS pointing, totaling 200 [OII] emitters per FMOS pointing. For Ly$\alpha$ emitters, we estimate that bright LAEs with $NB387 = 23.2$ have an H$\beta$ flux of $\simeq 4 \times 10^{-17}$ and [OII] or [OIII] fluxes of $\simeq 10 \times 10^{-17}$erg s$^{-1}$cm$^{-2}$ based on local young starbursts (Atek et al. 2008, A&A, 488, 491; Moustakas et al. 2006, ApJ, 642, 775; Nagao et al. 2006, A&A, 459, 85). LAEs of target-1 and target-2 sample are about 20 and 100 per FMOS pointing, respectively. The sample C is also selected by the criterion that emission-line flux is larger than $4.2 \times 10^{-17}$ erg s$^{-1}$cm$^{-2}$. We have $> 160$ target-2 in the sample C per FMOS pointing.

From our stacking analysis, we will detect H$\beta$ lines with fluxes of $1.4\times10^{-17}$ ($7\times10^{-18}$) erg s$^{-1}$cm$^{-2}$ with S/N=10 for [OII] emitters (LAEs) in composites of 40 (300) target-2 spectra. The number of target-2 [OII] emitters is large enough to investigate metal abundance, dust extinction, and star-formation rate as a function of stellar mass and equivalent width based on composite spectra made from several different subsamples.

In order to detect emission lines with $4.2(2.9) \times 10^{-17}$ erg s$^{-1}$cm$^{-2}$ in a S/N of 5, we need a 2.8(5.7)-hour on-source integration at each spectral coverage in the HR mode for [OII] emitters (LAEs). Since LAEs are fainter than the other emitters on average, a deeper 5.7-hour on-source integration is required. Taking overhead of 40% into account, the required times are 4.0(8.0) hours for our observations of [OII] emitters (LAEs). We will conduct the observation with the cross beam switching mode. By arranging the fibre allocation among samples properly, we can save the machine time much.

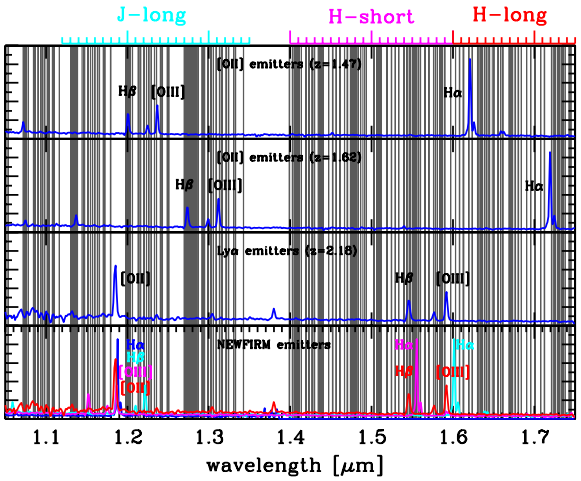


Figure 14 Template spectra of star-forming galaxy shifted to the redshift of emitters, respectively (Kinney et al., 1996, ApJ, 467, 38). Cyan, magenta, and red regions on the upper horizontal axis show the wavelength coverage of "J-long", "H-short" and "H-long" in the HR mode, respectively. The gray regions denote OH airglow masks of FMOS. HiZELS sources (sample D) are the emitters detected in gaps of OH airglow emissions; at 1.21 $\mu$m, 1.62 $\mu$m, and 2.12$\mu$m (out of the figure).

Since two spectral coverages in the HR mode are required for each target, we will perform two sets of observations at the same position but with different wavelength coverages. Therefore, at one position, 8 (= 4 hours $\times$ 2 bands $\times$ 1 pointing ) hours are required for observations of sample A, while $16(= 8 \times 2 \times 1)$ hours for sample B and C.

In SXDS, since we need 5 pointings for sample A and 4 pointings for sample B and C, $8 \times 5 = 40$ hours and $16 \times 4 = 64$ hours, respectively, are necessary. Considering weather factor of 0.75, a total 139 h or 17.3 nights are necessary. In COSMOS, 1 pointing is necessary both for sample B and C. So $16/0.75 = 21.3$ hours or 2.7 nights are required. In the supplementary fields of CDF-S and SDF, sample B+C and A in one FoV are the targets, and 2.7 and 1.3 nights are necessary, respectively.

Detection flux level of sample D is $\approx 1.0 \times 10^{-16}$ erg s$^{-1}$cm$^{-2}$ at each redshift. One of advantages to use sample D is the targets have guaranteed emission lines in the J and H bands, respectively. While the NB$_K$ targets at $z = 2.23$ emitters should show [OII] and H$\beta$ lines. For H$\alpha$ emitters, as like the other emitters, employing HR mode would be suitable. Supposing the limiting H$\alpha$ flux of $1.5\times10^{-16}$ erg s$^{-1}$ cm$^{-2}$ and considering the expected H$\beta$ flux is $\sim \frac{1}{3}$ of it, we like to detect such a line with S/N of 5. To achieve this, 2 h on-source time (4 h including overhead and clear night fraction) is necessary. Since the number of targets in FMOS one pointing is $\sim$200 in JL mode, $\sim$ 100 in HL/HS mode (assuming we can take spectra between HL and HS),

8 hours are necessary in one FMOS FoV. Among the 7 fields, we select two deep well-studies fields here: UDS and COSMOS. At least three and four FMOS pointings are necessary in UDS/SXDS and COSMOS, respectively. Thus $8 \times 3 = 24$h or 3 nights and $8 \times 4 = 32$h or 4 nights are required to UDS/SXDS and COSMOS, respectively.

Table 3 Summary of narrow-band emitter targets. Narrow-band filters used, emission line detected, redshift of targets, the number of targets per FMOS pointing and camera set-up in the HR mode are shown. Target-1 consists of bright emitters is detectable on an individual galaxy basis. Target-2 is used for faint emitters from which we expect to detect any of the major nebular lines. NB921 and NB973 data are available in the SDF and SXDS fields, while NB387 and NB119 are available in the SXDS, COSMOS, and CDFS fields. HiZELS samples in SXDS/UDS and COSMOS will be used.

| Emitter sample | Narrow-band filter | | Emission line | Redshift | Number of target | camera set-up |
|---|---|---|---|---|---|---|
| | filter | $\lambda_c$[Å]/$\Delta\lambda$[Å] | | | target-1/target-2 | |
| [O II] emitters | NB921 | 9193/133 | [O II] | 1.47 | 40/150 | J-long, H-long |
| | NB973 | 9755/202 | [O II] | 1.62 | 14/– | J-long, H-long |
| Ly$\alpha$ emitters (LAEs) | NB387 | 3871/94 | Ly$\alpha$ | 2.18 | 20/100 | J-long, H-short |
| NEWFIRM emitters | NB119 | 11866/111 | H$\alpha$, [O III]<br>H$\beta$, [O II] | 0.81-2.18 | –/160 | J-long, H-short |
| H$\alpha$ emitters (HiZELS) | NB$_J$ | 12100/150 | H$\alpha$ | 0.84 | $\sim$ 140/– | J-long |
| | NB$_H$ | 16210/180 | H$\alpha$ | 1.47 | $\sim$ 90/– | J-long, H-long |
| | NB$_K$ | 21210/210 | H$\alpha$ | 2.23 | $\sim$ 80/– | J-long, H-long/short |

## 5.5 Extend-sample 4: Dusty star-forming galaxies (MIR/FIR/submm sources)

Because heavily observed galaxies are faint even in the near-infrared bands, such galaxies can be missed in the above selections. In order to extend the sample to heavily obscured galaxies, we supplement the sample with galaxies selected from MIR in the *AKARI* survey in the NEP field, with sub-mm emission in the ASTE/AzTEC survey in the SXDS, and with FIR emission in the HERMES survey with *Hershel*. Sub-mm and FIR selections of galaxies is crucial to pick out dusty star-forming galaxies in the peak epoch. Continuous MIR coverage of *AKARI* data is important to understand dust properties of dusty galaxies.

### 5.5.1 AKARI sources in AKARI Deep Field (NEP) − synergy with *AKARI*

A sample from *AKARI* NEP-Deep survey has an advantage to study properties of dust obscuration. The area of 0.4 deg$^2$ near the north ecliptic pole (NEP) was observed with *AKARI*/InfraRed Camera (IRC) with continuous wavelength coverage from 2 to 24 $\mu$m (Fig 3).

We prepare the following samples from the *AKARI* NEP-Deep survey. The main characteristic of these samples is that we have direct measurements of the rest-frame 8 $\mu$m luminosity of these galaxies. In this program, we concentrate on the sub-field of the NEP-Deep survey where deep optical images have been obtained with Subaru/S-cam.

**A – All-band detected galaxies:** galaxies in this sample are detected in all of AKARI/IRC bands, except for the shallow 24 $\mu$m band. This sample satisfies the following selection criteria – **1)** Detected in all of 2,3,4,7,9,11,15 and 18 $\mu$ms with more than $3\,\sigma$, but should be detected with $> 5\,\sigma$ in at least one of the mid-IR bands; **2)** Red in near-IR ($N2 - N3 > -0.4$). This effectively excludes low-$z$ galaxies. There are 532 such objects in the S-cam field.

**B – 15 and 18 $\mu$m detected galaxies at $z \sim 1$:** Among the IRC-detected galaxies, sample A is somewhat biased to relatively bright sources. In order to increase the sample size at $z \sim 1$, we select additional galaxies as follows – **1)** Galaxies with $0.8 < z_{photo} < 1.5$; **2)** that are detected in both 15 and 18 $\mu$m bands with $> 5\,\sigma$; **3)** Red near-IR colour ($N2 - N3 > -0.4$). The total number of galaxies in this additional sample is 212.

**C – MIR-faint (low $A_V$) galaxies:** In order to investigate the properties of dust extinction, it is necessary to analyze a sample with a large dynamic range in $A_V$. Since the mid-IR detected galaxies in sample A and B are likely to be biased to higher $A_V$, we include galaxies which are not detected in the rest-frame 8 $\mu$m, and are therefore expected to have low $A_V$. The selection criteria are as follows – **1)** Not detected in the rest-frame 8 $\mu$m (based on photo-$z$); **2)** Estimated SFR from SED fitting $> 5\,M_\odot$ yr$^{-1}$; **3)** $A_V < 0.5$ estimated from SED fitting. There are $\sim$800 such galaxies in the S-cam field, of which we select $\sim$300 galaxies to supplement our sample. These galaxies can be used to fill the fibers for each FMOS configuration, because of their high surface density.

Thus, we aim to observe $\sim 1100$ objects in total, which is large enough to conduct meaningful statistical analysis. We need 6 FMOS configurations to observe all of the targets in this sample. We estimate that H$\alpha$ emission lines can be detected for most of mid-IR detected targets with a sensitivity of $5 \times 10^{-17}$ erg s$^{-1}$ cm$^{-2}$, assuming IR-derived SFRs, an average extinction of $A_V = 1.25$ for the stellar continuum, and the differential extinction taken from Calzetti (1997). This requires the on-source integration of 4 hours with FMOS. By considering the overheads for the cross-beam switching mode and weather conditions, we estimate that 6 nights of observation will be required for the NEP-Deep area.

### 5.5.2 Submm sources − synergy with ASTE/AzTEC

In ASTE/AzTEC $\lambda$ 1100 $\mu$m deep surveys, 206 robust ($> 3.5\sigma$) submm galaxies (SMGs) have been detected in SXDS ($\sim$ 960 arcmin$^2$) with a sensitivity of 0.4 - 0.8 mJy (1 $\sigma$) (Ikarashi et al., in prep.), which is sufficient to uncover ultra-luminous infrared galaxies at $z > 1.5$. This is the largest sample of SMGs selected at $\lambda \sim 1$ mm to date: wider than the SCUBA survey (Coppin et al. 2006, MNRAS, 372, 1621) and deeper than the JCMT/AzTEC survey (Austermann et al. 2009, MNRAS, 393, 1573). It is very complementary to the short wavelengths SMG surveys by *Herschel*/SPIRE (250 - 500 $\mu$m). Thanks to its superb capability of FMOS, it is expected to double (or triple depending on their redshift distributions) the number of SMGs with the rest-frame optical spectra, which are currently limited to just 20-30 objects (Swinbank et al. 2004, ApJ, 617, 64; Motohara et al. 2005, AJ, 129, 53; Takata et al. 2006, ApJ, 651, 713).

In the SXDS, about 100 of them have a near-infrared counterpart with the estimated H band magnitude of $H_{\rm AB} = 22 - 24$ mag. We calculate the expected H$\beta$ flux from SFR and E(B-V) obtained from SED fitting: Assuming the Kennicutt relation between SFR and H$\alpha$ luminosity, an H$\alpha$/H$\beta$ ratio of 2.87, the Calzetti extinction law, and a redshift of $\sim 2$, we find that emission line fluxes $> 5 \times 10^{-17}$ erg s$^{-1}$ cm$^{-2}$ will be expected, and these are detectable with S/N $> 5$ after an on-source time of 4 hours. Including time for calibrations etc., we need 1 clear night for SXDS observations.

SMGs in SXDS were/are observed during open use/GTO, but we have further samples of SMGs in other blank fields (SDF, COSMOS, and CDF-S) and in the biased regions/clusters listed in Table 4 (SSA 22, 4C23.56, PKS 1138-262, XCS2215.9-1738, and RXJ0152-1357) (Tamura et al. 2009, Nature, 459, 61; Scott et al. 2010, MNRAS, 405, 2260; etc). These fields also provide another $\sim 480$ SMGs, about half of which, i.e., $\sim$ 240 sources, will have a NIR counterpart which is suitable for FMOS observations. Since the number density is not so high in the FMOS FOV (typically $\sim$ 100 targets per fov), many of these targets can be observed as extra allocations within observations of these fields for other target samples, depending on the availability of fibers and observing seasons.

### 5.5.3 HERMES sources − synergy with *Herschel*

Among the *Herschel* Multi-tiered Extragalactic Survey (HERMES) sources detected at 250$\mu$m with $> 20$ mJy in the COSMOS field, optical/NIR counterparts are identified with the help of NIR and *HST*/ACS images. We further restrict the sample with $z_{\rm phot} = 1 - 2$ using multiband photometry data, leading $\sim$ 200 sources/FoV and in total $\sim$ 800 sources (4 pointings). The expected H$\alpha$ flux is $\gtrsim 1 \times 10^{-16}$ erg s$^{-1}$ cm$^{-2}$, and the GTO observations show fairly large fraction of them show such an emission-line. Thus the exposure time of 1 h would be good enough and the observing time of 2 hour is needed for one FoV. Thus with 8 h (= 1 night), we can observe $\sim 800$ HERMES sources in the COSMOS field.

## 5.6 Extend-sample 5: Active galaxies

AGNs are important to understand not only SMBH growth but also galaxy evolution, and unveiling AGN evolution is another key for this program. Although part of AGNs can be selected with the above core-sample, mass-limited extend sample 2, or MIR/FIR selected sample 4, mildly-obscured and non-obscured AGNs can be efficiently selected with X-ray and radio selections.

### 5.6.1 X-ray selected sources

Samples of non-obscured and mildly-obscured AGNs are constructed based on X-ray selection. In order to construct samples with sufficient number of AGNs at deep flux limit, we selected wide X-ray survey fields with multiwavelength datasets, i.e. SXDS and COSMOS as target fields. In the two fields, multiwavelength datasets which are crucial to examine completeness of X-ray AGN selection and to evaluate properties of host galaxies are available from UV (GALEX) to MIR/FIR (*Spitzer*, *Herschel*). In these fields, intensive optical spectroscopic observations have been done, and optically-bright objects are spectroscopically identified, but there are significant number of optically-faint X-ray sources and they have not been identified. For example among the 900 X-ray sources detected in the SXDS region, there are 500 X-ray sources which have no spectroscopic redshift information. Based on photometric redshifts, 280 of the 500 sources have $z_{\rm ph} = 1.0 - 2.6$ and at least one emission line is expected in the FMOS spectroscopic window. These 280 sources are our primary targets, with 220 secondary targets. All of the primary targets will be observed, and secondary targets are observed serendipitously (i.e. assigned a low priority). The sample is selected as $K_{\rm AB} < 23.9$ mag. About 8 hours integration per target is required to achieve high identification rate. Part of the optically-unidentified X-ray sources are observed in the course of the guaranteed time observation of FMOS team, and in order to cover the remaining X-ray sources, we require 3 fovs, therefore in total, 3 FoVs x 11.2 hours (incl. overhead) / 0.75 (weather) = 44.8 h = 5.6 nights

To enlarge the sample size and to include areas with *HST* imaging (which may be helpful for studying co-evolution), we add the COSMOS field and supplementary CDF-S.

COSMOS: 2 fovs $\times$ 11.2 hours (incl. overhead) / 0.75 (weather) = 29.9 h = 3.7 nights

CDF-S: 1 fov $\times$ 11.2 hours (incl. overhead) / 0.75 (weather) = 14.9 h = 1.9 nights

Note that the number density of the primary targets is 50-60/FOV, and thus they can be observed in parallel with other targets samples.

### 5.6.2 Radio selected sources

We have selected radio sources in the SXDF/UDS (from a new radio map; Ivison et al., in prep) which are believed to lie at $z > 1.3$, based on their *Spitzer* [3.6]−[4.5] colours. This colour cut will also include lower redshift 'quasar mode' AGN (due to the hot dust emission from the inner walls of the torus) and these objects have been excluded based on their optical magnitudes. There are 750 sources, with a range of $J$-band magnitudes, that therefore require different exposure times (from 2–36 hours in low-resolution mode). We aim to achieve S/N=5 in the continuum, which will be sufficient to detect the strong 4000-Å break. The total time request is 8400 fibre-hours, or $8400/200 \times 1.5/0.75 = 84$ hours (or 10.5 nights). We note that a part of the brighter sources should also be in the core-sample etc, and therefore 2.5 nights of this time has already been accounted for.

## 5.7 Extend-sample 6: Clusters

This sample is employed to study environmental (local density) effects on galaxy and AGN evolution covering from dense cluster core to general field. Kodama et al. (2005, PASJ, 57, 309; 2007, MNRAS, 377, 1717) have been conducting a panoramic study of distant clusters and their surrounding regions with Subaru (PISCES and HzRG) by utilizing its unique wide-field instruments both in the optical (Suprime-Cam) and in the near-infrared (MOIRCS). They have mapped out large scale structures (LSS) in and around ∼10 X-ray clusters at $0.39<z<1.62$ initially based on phot-$z$, with subsequent spectroscopic confirmation of many many of the structures (e.g. Tanaka et al. 2006, MNRAS, 365, 139). Seven proto-clusters discovered around high-$z$ radio galaxies have also been targeted and mapped out with MOIRCS. These structures serve as unique and ideal sites for environmental studies over a wide redshift range, as they cover virtually all possible environments at every epoch from the richest cluster cores which tend to be missed in blank field surveys, all the way to low density regions comparable to general fields.

Narrow-band imaging data are particularly useful for selecting target galaxies for FMOS spectroscopy as we already know which galaxies would have detectable emission lines. Also we will be able to compare our results in clusters and their surrounding regions with those in the general blank field surveys in SXDF and SDF where we have many comparable targets of narrow-band emitters (§ 2.1.3). For examples of the existing narrow-band surveys, [OII] emitter candidates over the Suprime-Cam fields in RXJ1716 ($z = 0.81$) and XCS2215 ($z = 1.46$) clusters are shown in Fig. 7. They are distributed over the entire fields, and provide excellent targets for the proposed FMOS spectroscopy. A pilot FMOS observation of these two clusters was performed in Jun 2010 as an open-use program. Although only low-resolution mode and ∼200 fibres were available at that time, more than 30 H$\alpha$ emitters in RXJ1716 were successfully identified. For XCS2215, we failed to detect any reliable H$\alpha$ emitters in the H-band where we suffered from remaining OH sky lines and in the low-resolution mode due probably to OH mask miss-alignment. The problem will be solved by the start of the SSP, and the high-resolution mode will also be available. We will re-observe these two core targets intensively in the proposed SSP. For the clusters without narrow-band imaging data, but showing confirmed prominent structures, such as RDCS1252, we will target the members already confirmed by optical spectroscopy and the phot-$z$ members spread over the FMOS field.

Our cluster targets are summarized in Table 4. Kodama et al. have now been awarded a Subaru intensive program (10 nights over the two semesters: S10B and S11A) named "MAHALO-Subaru" project (MApping HAlpha and Lines of Oxygen with Subaru), and we will conduct and complete NB imaging for higher-$z$ clusters, namely, CIGJ0218 ($z$=1.62; [OII] with Suprime-Cam), PKS1138 ($z$=2.16; H$\alpha$ with MOIRCS), and 4C23.56 ($z$=2.52; H$\alpha$ with MOIRCS). We will target the lower-$z$, but richest cluster CL0016 ($z$=0.55; H$\alpha$ with Suprime-Cam) as well.

We will use the high resolution mode (R=2200) of FMOS in order to gain higher sensitivity and to securely separate [NII] from H$\alpha$, and to measure dynamical masses of galaxies. Therefore, we need two wavelength settings for many of the targets to obtain all the important lines as listed in Table 4. Most of the target galaxies at $z > 0.8$ typically have a size of $1''$ and fit within a fibre with a diameter of $1.2''$. Our primary targets within each cluster field are emission line galaxies (where NB data are available) or blue member galaxies (based on spec-$z$ or phot-$z$), but we will also target "red" member candidates for the remaining fibres and we will stack the spectra in the same environmental bins so that we can obtain the averaged information on continua and absorption lines (such as H$\beta$ and H$\gamma$). We will also take two fibre configurations each per pointing in order to sample target galaxies as completely as possible even in the crowded regions. For CL0016 we need 3 pointings (i.e. 6 configurations) to cover even larger scale structures traced by 3 Suprime-Cam pointings. For emission lines, we have assumed that we can detect the line flux of $1 \times 10^{-16}$ erg s$^{-1}$ cm$^{-2}$ at $5\sigma$ with 1 hour net integration time according to the FMOS sensitivities. We will use the Kennicutt calibrations (1998) to convert from H$\alpha$ ([OII]) line intensities into star formation rates, with a dust extinction correction based on Balmer-decrement measurements, where these are available.

The required exposure times and the dust-free star formation rates of individual clusters are listed in Table 4. With 1–5 hrs integrations, we can reach down to 1–6 M$_\odot$ yr$^{-1}$ based on H$\alpha$, and we will be sensitive not only to star bursting galaxies but also to normal star forming galaxies. For the higher redshift sample at $z > 2.6$, we will rely on star formation rates solely measured from [OII] intensities, and we will reach to 15 to $38 M_\odot$ yr$^{-1}$ at $2 < z < 3$ with 10 hrs integration, allowing any strong star formation to be detected even at these high redshifts. Note that we aim to target these clusters with ALMA in the future in order to derive the molecular gas mass in these star forming galaxies. The star formation rates we can reach with FMOS are just comparable to the gas mass measured from CO($3 \rightarrow 2$) emissions within a reasonable amount of ALMA observing time ($\sim$ a few hours). We will also detect [NII], H$\beta$, and [OIII] lines for a part of our sample. The typical observed flux ratios of these lines to H$\alpha$ are 1/3, 1/5 and 1/6, respectively, for local star forming galaxies in SDSS (Moustakas et al. 2006, ApJ, 642, 775). For clusters at $z < 0.85$, we will concentrate on H$\alpha$ and [NII] lines in $J$-band, and for clusters at $1 < z < 2.6$ we will capture many emission lines, H$\beta$ and [OIII] lines in $J$-band, and H$\alpha$, [NII] lines in $H$-band, respectively.

Table 4 The list of our target clusters. Eight primary targets are shown by bold fonts. The targets are classified into 8 groups according to redshifts; $z \sim 0.55$, 0.8, 1.2, 1.4, 1.6, 2, 2.5, and 3, as separated by horizontal lines. These correspond to the look-back times of 5.4, 6.9, 8.5, 9.1, 9.6, 10.4, 11.1, and 11.6 Gyrs, respectively. We will use higher resolution mode (R=2200) and the number of configurations and the spectral coverages are shown in the table (Js, Jl, Hs, and Hl indicate J-short, J-long, H-short, and H-long, respectively.) Note that we have narrow-band emitter survey data for most of the primary targets, which provide excellent spectroscopic targets for FMOS. Ly$\alpha$ emitter surveys are also available for most of the higher-$z$ targets at $z > 2$. Note also that all of our targets, except for two (1716 and 0848), are visible from ALMA for future coordinated observations.

| Cluster | $z$ | Lx44 | NB | $M_\odot$/yr ($5\sigma$) | cfg. | spectra | expected lines | imaging |
|---|---|---|---|---|---|---|---|---|
| **CL 0016+1609** | **0.55** | 26.0 | H$\alpha$ | **1.0 (1hr)** | **6** | Js | H$\alpha$,[NII] | $BVRi'z'$ |
| MS 0451.6−0305 | 0.55 | 12.0 | — | 1.0 (2hr) | 2 | Js | H$\alpha$,[NII] | $BVRI$ |
| **RX J1716.4+6708** | **0.81** | 2.7 | H$\alpha$, [OII] | **1.7 (2hr)** | **2** | Jl | H$\alpha$,[NII] | $VRi'z'JK$ |
| RX J0152.7−1357 | 0.84 | 16.0 | — | 1.9 (2hr) | 2 | Jl | H$\alpha$,[NII] | $VRi'z'K$ |
| **RDCS J1252−2927** | **1.24** | 6.6 | — | **3.2 (5hr)** | **2** | Hs,Js | H$\alpha$,[NII],[OIII],H$\beta$ | $VRi'z'K$ |
| RX J0848.9+4452 | 1.26 | 2.8 | — | 3.3 (5hr) | 2 | Hs,Js | H$\alpha$,[NII],H$\beta$ | $BVRi'z'JK$ |
| XMM2235.3−2557 | 1.39 | 3.0 | — | 4.2 (5hr) | 2 | Hs,Jl | H$\alpha$,[NII],[OIII],H$\beta$ | $VRi'z'JK$ |
| **XCS2215.9−1738** | **1.46** | 4.3 | [OII] | **4.7 (5hr)** | **2** | Hl,Jl | H$\alpha$,[NII],[OIII],H$\beta$ | $BRi'z'K$ |
| CL0332−2742 | 1.61 | — | [OII] | 6.0 (5hr) | 2 | Hl,Jl | H$\alpha$,[NII],[OIII],H$\beta$ | $BVizJHK$ |
| **CIGJ0218.3−0510** | **1.62** | 3.4 | [OII] | **6.1 (5hr)** | **2** | Hl,Jl | H$\alpha$,[NII],[OIII],H$\beta$ | $BVRi'z'JHK$ |
| **PKS 1138−262** | **2.16** | — | H$\alpha$, Ly$\alpha$ | **15 (10hr)** | **1** | Hs,Jl | [OII],[OIII],H$\beta$ | $BVRIJHK$ |
| **4C 23.56** | **2.48** | — | H$\alpha$ Ly$\alpha$ | **22 (10hr)** | **1** | Hl,Jl | [OII],[OIII],H$\beta$ | $Bz'JHK$ |
| USS 1558−003 | 2.53 | — | H$\alpha$ | 23 (10hr) | 1 | Hl,Jl | [OII],[OIII],H$\beta$ | $Bz'JHK$ |
| USS 0943−242 | 2.92 | — | Ly$\alpha$ | 32 (10hr) | 1 | Hs | [OII] | $VIJHK$ |
| **SSA22** | **3.09** | — | Ly$\alpha$ | **37 (10hr)** | **1** | Hs | [OII] | $BVRi'z'JHK$ |
| MRC 0316−257 | 3.13 | — | Ly$\alpha$ | 38 (10hr) | 1 | Hs | [OII] | $BVRIJHK$ |

Including a ∼40% overhead with beam switching for each configuration, the total requested time to complete this part of the programme amounts to 200 hrs or 20 nights for the 8 primary targets. For the 8 secondary targets, we would like to observe them if we can have observing chances. These numbers could change by ∼30% depending on the actual efficiency of fibre allocation and the type of appropriate beam switching that will actually be used for each cluster.

# 6 Required nights and a plan for allocation

Total nights necessary to conduct this SSP is 122 (108.5 for the main fields and 13.5 for the supplementary fields). The observing fields and required nights for each field are summarized in Table 2 and Table 5. (Required nights include overhead of 40–50% and clear night fraction of 75–80%.) Considering the distribution of right ascensions of the fields as well as telescope down time and other SSP program to some extent, we show a rough plan for allocation in Table 6. Of course this is a plan, and the actual scheduling should be made with Subaru observatory.

# 7 Organization of FMOS SSP

The organization of the SSP consortium has been under discussion since Jan. 2006, in parallel with the late stages of the instrument development. Initially this was considered as an extension of GTO time into large programmes, there being no SSP framework at that time. Since the SSP framework was established during the FMOS commissioning phase we have intensified these discussions with several international meetings and performance inputs based on on-sky measurements from engineering observations.

In order to pursue the SSP with FMOS, we have established three science groups as follows: Evolution of galaxies in the general field (Group 1), Evolution of AGN/QSOs (Group 2), and The effect of environment on evolution (Group 3). Each group considers their own program rather autonomously, but regular discussions ensure close connections and well organized studies among the groups. Specific aims within a group may call for the development of subgroups if this provides a more efficient path to achieving the scientific aims.

## 7.1 Groups and members

The PI is Kouji Ohta, Department of Astronomy, Kyoto University. The Co-PI is Naoyuki Tamura, Subaru Telescope, NAOJ. Andrew Bunker, University of Oxford, UK, is the UK representative (in this sense, referred as Co-PI below). One or two post-docs will be joining at Hilo, to assist with target assignment to fibres, survey management, observing runs, data reduction, etc. One will be employed by Subaru. The FMOS consortium will make an effort to employ one more post-doc class researcher using

Table 5. Summary for fields, samples, and required nights.

| Field | Sample | Sample detail | Number | Mode | Nights[1] | Science key words |
|---|---|---|---|---|---|---|
| **Galaxy and AGN evolution in general fields** | | | | | | |
| **SXDS/UDS** | core | stellarmass&flux limit sample | ∼3200 | LR | 14.4 | SFR,extinction,metallicity, extinction,AGN fraction |
| | Ext-sample 1 | stellarmass limit sample | $\sim 1800$ | LR | 5.4 | SFR,metallicity, Compton thick AGNs |
| | Ext-sample 2 | pBzKs | $< 50$ | LR | −[2] | stellar population |
| | Ext-sample 3 | [OII] emitters (SCam) ($z = 1.47, 1.62$) | $\sim 1000$[3] | HR (JL,HL) | 6.6 | SFR,extinction,metallicity, gas kinematics |
| | | LAEs (SCam) ($z = 2.18$) | $\sim 480$[2] | HR (JL,HS) | 6.4 | SFR,extinction,metallicity, gas kinematics |
| | | [OII],H$\beta$,[OIII],H$\alpha$ emitters (NEWFIRM) | $\sim 640$[3] | HR (JL,HS) | 4.2 | SFR,extinction,metallicity, gas kinematics |
| | | H$\alpha$ emitters (HiZELS) ($z = 0.8, 1.5, 2.2$) | $\sim 900$ | HR (JL,HS/HL) | 3 | SFR,extinction,metallicity, gas kinematics |
| | Ext-sample 4 | AzTEC sources | $< 100$ | LR | − | obscured SFR |
| | Ext-sample 5 | X-ray sources | 280(+220) | LR | 5.6 | AGNs(non-/obscured) |
| | | VLA sources | 750 | LR | 8 | AGNs, feedback |
| **COSMOS** | core | stellarmass&flux limit sample | $1500 \sim 2000$ | LR | 15 | SFR, metallicity, extinction,AGN fraction |
| | | stellar mass limit w/ $z_{\rm spec}$ | $\sim 600$ | HR (JL,HL) | 2.5 | SFR,extinction,metallicity, gas kinematics |
| | Ext-sample 2 | pBzKs | $< 50$ | LR | − | stellar population |
| | Ext-sample 3 | LAEs (SCam) ($z = 2.18$) | $\sim 120$[3] | HR (JL,HS) | 1.6 | SFR,extinction,metallicity, gas kinematics |
| | | [OII],H$\beta$,[OIII],H$\alpha$ emitters (NEWFIRM) | $\sim 160$[3] | HR (JL,HS) | 1.1 | SFR,extinction,metallicity, gas kinematics |
| | | H$\alpha$ emitters (HiZELS) ($z = 0.8, 1.5, 2.2$) | $\sim 1200$ | HR (JL,HS/HL) | 4 | SFR,extinction,metallicity, gas kinematics |
| | Ext-sample 4 | AzTEC sources | $< 100$ | LR | − | obscured SFR |
| | | HERMES sources | $\sim 800$ | LR | 1 | obscured SFR |
| | Ext-sample 5 | X-ray sources | $\sim 200$ | LR | 3.7 | AGN(non-/obscured) |
| | | VLA sources | as many | LR | − | AGNs, feedback |
| **AKARI Deep Field** | Ext-sample 4 | AKARI sources | $\sim 1100$ | LR | 6 | obscured SFR, extinction |
| **Galaxy and AGN evolution in dense environment** | | | | | | |
| **Clusters** | see Table 4 | star-forming galaxies | - | HR (JS-HL) | 20(+20) | environment effects on galaxy/AGN evolution |
| **Supplementary fields** | | | | | | |
| **CDF-S** | core | stellar mass limit w/ $z_{\rm spec}$ | $\sim 400$ | HR (JL,HL) | 2 | SFR,extinction,metallicity, gas kinematics |
| | Ext-sample 3 | LAEs (SCam) ($z = 2.18$) | $\sim 120$[3] | HR (JL,HS) | 1.6 | SFR,extinction,metallicity, gas kinematics |
| | | [OII],H$\beta$,[OIII],H$\alpha$ emitters (NEWFIRM) | $\sim 160$[3] | HR (JL,HS) | 1.1 | SFR,extinction,metallicity, gas kinematics |
| | Ext-sample 4 | AzTEC/LABOCA sources | $\sim 100$ | LR | − | obscured SFR |
| | Ext-sample 5 | X-ray sources | $\sim 100$ | LR | 1.9 | AGN(non-/obscured) |
| **Subaru Deep Field** (SDF) | core | stellarmass&flux limit sample | $\sim 880$ | LR | 3.6 | SFR,metallicity, extinction,AGN fraction |
| | Ext-sample 3 | [OII] emitters (SCam) ($z = 1.47, 1.62$) | $\sim 200$[3] | HR (JL,HL) | 1.3 | SFR,extinction,metallicity, gas kinematics |
| **AEGIS** | core | stellar mass limit w/ $z_{\rm spec}$ | $\sim 400$ | HR (JL,HL) | 2 | SFR,extinction,metallicity, gas kinematics |

[1]Required nights include overhead of 40-50% and clear night fraction of 75-80%.

[2]No number of nights assigned because of parasite-observation

[3]Number include target 1 and target 2.

Table 6 The number of required nights in semesters from S11B to S16A (TBD). The numbers in parenthesis indicate the required nights for the supplementary fields, which is NOT included in the numbers for the primary fields (outside parenthesis). We request 108.5+13.5=122 nights in total.

| Field | S11B | S12A | S12B | S13A | S13B | S14A | S14B | S15A | S15B | S16A | Total |
|---|---|---|---|---|---|---|---|---|---|---|---|
| **SXDS/UDS** (CDF-S) | 9.6 | | 12(2.6) | | 12(2) | | 10(2) | | 10 | | 53.6(6.6) |
| **COSMOS** (SDF, AEGIS) | | 7(2.9) | | 7(2) | | 7 | | 7 | | 0.9 | 28.9(4.9) |
| **ADF** (SDF, AEGIS) | | 2(2) | | 2 | | 2 | | | | | 6(2) |
| **Clusters** | | 3 | 3 | 2 | 2 | 2 | 2 | 2 | 2 | 2 | 20 |
| **Total** | 9.6 | 12(4.9) | 15(2.6) | 11(2) | 14(2) | 11 | 12(2) | 9 | 12 | 2.9 | **108.5(13.5)** |

such as Kakenhi (grant). UK funds are outlined for on post-doc in Oxford to assist with the survey execution. A (or a few) senior grad student(s) may take this role. There are some candidates in Japan and UK.

Number of the FMOS consortium members is 54 as of the proposal submission: 35 Japanese (in Japanese institutes and Japanese in foreign institutes (same as the Subaru policy)), 15 UK astronomers, and 4 in other institutes (see list below). (Note: the 3rd category members are basically 'liaison' persons connecting SSP members and his/her collaborating group outside the FMOS consortium.)

Before the SAC approving, we plan to have a FMOS WS during Feb 28 to Mar 2 (2011). We intend to widen the consortium aiming at maximizing the scientific outputs in the current framework but without making a significant change to the structure and strategy of the survey.

Current members are as follows (PI joins all the groups):

Group 1: evolution of galaxies

1-1: star-forming galaxies

K. Yabe(Kyoto), M. Akiyama, T. Yamada(Tohoku), K. Motohara, M. Tanaka, M. Ouchi(Tokyo), M. Hayashi(NAO), N. Tamura, I. Iwata, T. Kodama(NAO Subaru), K. Tadaki(NAO/Tokyo), T. Nagao, M. Kajisawa(Ehime), T. Yoshikawa(Kyoto Sangyo), A. Bunker(Oxford), R. Bower(Durham), M. Onodera, S. Lilly(ETH), J. Silverman(Tokyo), A. Renzini (INAF–Padova), E. Daddi (CEA/Saclay)

1-2: star-forming low-mass galaxies (emitters)

M. Hayashi(NAO), M. Ouchi, K. Shimasaku, T. Hashimoto, Y. Ono, K. Nakajima(Tokyo), J. Lee(Carnegie Observatories), T. Yamada(Tohoku), Y. Matsuda(Durham), T. Kodama(NAO, Subaru), K. Tadaki (NAO/Tokyo), Y. Koyama (Tokyo/NAOJ), M. Tanaka(Tokyo), A. Bunker(Oxford), I. Smail(Durham), P. Best(Edinburgh), M. Jarvis(Hertfordshire)

1-3: AKARI sources

T. Takagi, H. Matsuhara(ISAS/JAXA), H. Hanami(Iwate), T. Ishigaki(Asahikawa NCT), N. Fujishiro (Kyoto Sangyo), S. Serjeant, G.J. White(Open Univ), C.P. Pearson(RAL), M. Akiyama(Tohoku)

1-4:submm(AzTEC/HERMES) sources

K. Kohno, S. Ikarashi, K. Motohara(Tokyo), K. Yabe(Kyoto), S. Oliver, I. Roseboom (Sussex), I. Smail (Durham)

1-5: passive galaxies

N. Tamura, T. Kodama(NAO Subaru), M. Hayashi(NAO), T. Yamada(Tohoku), M. Onodera(ETH), O. Almaini(Nottingham)

Group 2 evolution of AGNs (mass accretion onto SMBHs)

2-1: obscured AGNs including Compton thick AGNs

M. Akiyama, K. Nobuta, M. Fuji(Tohoku), T. Nagao(Ehime), Y. Ueda(Kyoto), J. Silverman(Tokyo)

2-2: non-obscured AGNs

M. Akiyama (Tohoku), Y. Ueda, F. Iwamuro(Kyoto), J. Silverman(Tokyo)

2-3: radio sources and elliptical galaxy formation

C. Simpson(LJMU), S. Rawlings(Oxford), J. Dunlop(Edinburgh), G. J. White (Open Univ), M. Akiyama(Tohoku)

Group 3 Environmental effect

3-1 star-forming galaxies

T. Kodama, N. Tamura, I. Tanaka(NAO Subaru), M. Hayashi(NAO), M. Tanaka, Y. Koyama(Tokyo), K. Tadaki(NAO/Tokyo), T. Yamada(Tohoku), Y. Matsuda, R. Bower, I. Smail, A. Edge(Durham)

3-2 AGNs

M. Akiyama(Tohoku), Y. Ueda(Kyoto)

### 7.2 Management of the consortium

We intend to hold regular consortium meetings (usually via video conference) every half year prior to each A/B semester to discuss the relative priorities of the input samples and science objectives to be made in the next semester. In the meeting, members will be watching and evaluating recent observational results. Each group has more small meetings, according to necessity.

Each group/subgroup input the samples and actual target selection will be made by 'core team' considering the discussion above. The team will be responsible for target selection and fibre assignment for SSP runs. This is because there are many ways to put targets in various scientific purposes, and determining the optimal strategy is complex. Further, the team also has to make an effort to take care of the 30% contribution of UK community to FMOS in accordance with the FMOS agreement. The core team consists of several members including PI, CoPIs, PDF(s) at Hilo, and a few experts from the FMOS instrument team.

Observing runs will be carried out by team consisting of members from sample input groups and from the core team. The FMOS instrument team from Kyoto and Oxford expects to support these observations.

We assume that the priority for the first data access and for writing papers goes to the members who input the sample. This is not only a right, but is also duty. The priority to the observed data will be one year (details are still under discussion). After that any consortium members are allowed to use the data and write further paper.

The authorship policy for papers is as follows: the members who input the sample, the collaborators of the group (consortium members or not), and the core team. The objective here is that the authors should be persons who contribute significantly to the success of the project, and not all the members of a large consortium.

We anticipate that the FMOS instrument team members have the right to request co-authorship of papers in which they have an established scientific interest.

## 8 Data reduction and analysis plan

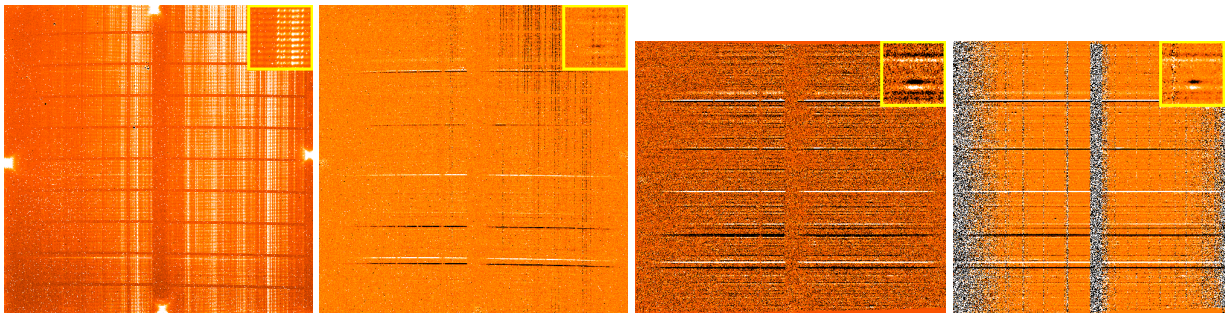

Figure 15 Spectral images before and after the reduction pipeline is applied. Left) raw image taken with IRS1 with 15min exposure, Left-center) after sky subtraction (cross-beam switch), Right-center) output image by combining 3 pairs of images after applying the pipeline reduction procedure, Right) wavelength and flux calibrated image (5Å/pix, 1$\mu$Jy/ADU). A partially-enlarged view is superimposed at the top-right of each image.

The data will be reduced to instrument-corrected, wavelength calibrated, sky-subtracted, flux-calibrated spectra using the pipeline software developed by Iwamuro (Kyoto) and colleagues. The software is now available for open use users, and it has been improving using data taken during engineering runs and open use runs. Quick look analysis during the observations is also available using this pipeline to provide a quality control measure prior to accepting data for release to the consortium. The final data produced with the pipeline will be supplied to the survey groups within one or two weeks after the observations. There is still a possibility that Anglo Australian Observatory develops FMOSDR (FMOS Data Reduction) software based on 2dFDR, but currently we are not dependent on FMOSDR.

The post-reduction data analysis should be done by each input group based on their scientific interests. Simulations are required to interpret the effect of the OH-suppression masks on the final sample statistics. We are developing such simulations to correct for the mask loss using actual data taken during GTO.

## 9 Archive policy

The raw data will be released to consortium members immediately after the observations, subject to quality control, based on Quick-look analysis made during the observations. The data will be reduced using the pipeline reduction software described above within a week or so. The reduced data will be supplied to the consortium (but with higher priority to the team in charge of the analysis). The 1.5 year rule of Subaru is applied to the data.

The final data products including target name, coordinates, photometric properties, spectroscopic properties obtained with FMOS (and other optical spectroscopy) will be made available on a web site for public use. This public release is expected to start in the later stage of SSP in a phased manner (i.e. 1-2 year after blocks of data are observed).